

# 1 Multi-fold increase in rainforests tipping risk beyond 1.5-2°C warming

2 Chandrakant Singh<sup>1,2,3,\*</sup>, Ruud van der Ent<sup>4</sup>, Ingo Fetzer<sup>1,2,5</sup>, Lan Wang-Erlandsson<sup>1,2,5</sup>

3 <sup>1</sup>Stockholm Resilience Centre, Stockholm University, Stockholm, Sweden

4 <sup>2</sup>Bolin Centre for Climate Research, Stockholm University, Stockholm, Sweden

5 <sup>3</sup>Department of Space, Earth and Environment, Chalmers University of Technology, Gothenburg, Sweden

6 <sup>4</sup>Department of Water Management, Faculty of Civil Engineering and Geosciences, Delft University of Technology, Delft,  
7 The Netherlands

8 <sup>5</sup>Potsdam Institute for Climate Impact Research, Potsdam, Germany

9

10 \*Corresponding author; E-mail: chandrakant.singh@su.se, chandrakant.singh@chalmers.se

11

## 12 ORCID

13 Chandrakant Singh: <http://orcid.org/0000-0001-9092-1855>

14 Ruud van der Ent: <https://orcid.org/0000-0001-5450-4333>

15 Ingo Fetzer: <http://orcid.org/0000-0001-7335-5679>

16 Lan Wang-Erlandsson: <http://orcid.org/0000-0002-7739-5069>

17

18 **Abstract.** Tropical rainforests rely on their root systems to access moisture stored in soil during wet periods for  
19 use during dry periods. When this root-zone soil moisture is inadequate to sustain a forest ecosystem, they  
20 transition to a savanna-like state, losing their native structure and functions. Yet the influence of climate change  
21 on ecosystem's root-zone soil moisture storage and their impact on rainforest ecosystems remain uncertain. This  
22 study assesses the future state of rainforests and the risk of forest-to-savanna transitions in South America and  
23 Africa under four shared socioeconomic pathways (SSP1-2.6, SSP2-4.5, SSP3-7.0, and SSP5-8.5). Using a mass-  
24 balance-based empirical understanding of root zone storage capacity ( $S_r$ ), defined as the maximum volume of  
25 root zone soil moisture per unit area accessible to vegetation's roots for transpiration, we project how rainforest  
26 ecosystems will respond to future climate changes. We find that under the end-of-the-21<sup>st</sup>-century climate, nearly  
27 one-third of the total forest area will be influenced by climate change. As the climate warms, forests will require  
28 a larger  $S_r$  than they do under the current climate to sustain their ecosystem structure and functions, making them  
29 more ~~susceptible to water limitations~~. ~~water-limited~~. ~~Meanwhile, recovering to a less water-limited state gradually~~  
30 ~~diminishes~~. Furthermore, warming beyond 1.5-2°C will significantly elevate the risk of a forest-savanna  
31 transition. In the Amazon, the forest area at risk of such a transition grows by about 1.7-5.8 times in size compared  
32 to the ~~the~~ immediate lower warming scenario (e.g., SSP2-4.5 compared to SSP1-2.6). In contrast, the risk growth  
33 in the Congo is less substantial, ranging from 0.7-1.7 times. These insights underscore the urgent need to limit  
34 ~~global surface temperature rise~~ the rise of global surface temperature below the Paris Agreement to conserve  
35 rainforest ecosystems and associated ecosystem services.

## 36 1 Introduction

37 Tropical rainforests in the Amazon and Congo basins are critical to the Earth system since they store and  
38 sequester a large amount of carbon, host vast biodiversity, and regulate the global water cycle (Malhi et al., 2014).  
39 However, these forests are under severe pressure from climate ~~change~~ and land-use changes (Davidson et al.,  
40 2012; Lewis et al., 2015; Malhi et al., 2008), ~~which risk amplifying further warming and forest degradation~~  
41 ~~(Lawrence et al., 2022). These changes~~ Climate change and land-use change result in decreased precipitation,  
42 ~~increased seasonality, and higher atmospheric water demand lead to a decrease in precipitation, an increase in~~  
43 ~~seasonality and atmospheric water demand (Malhi et al., 2014). (Malhi et al., 2014), leading to~~ This causes a  
44 ~~deficit in~~ soil moisture ~~deficits~~ availability that inhibits plant growth (Singh et al., 2020; Wang-Erlandsson et al.,  
45 2022). Furthermore, ~~climate-induced hydroclimatic changes, including the~~ projected increases in drought  
46 frequency, severity, and duration ~~under future climate change~~ (Dai, 2011; Liu et al., 2018), ~~present pose~~ imminent  
47 threats to the capacity of rainforests to maintain their native ecological structure and functions (i.e., forest  
48 resilience) (Bauman et al., 2022; Grimm et al., 2013; Jones et al., 2009).

49 Under water-deficit conditions, rainforests adapt by investing in their root systems to gain better access to  
50 soil moisture necessary to maintain their structure and functions (Singh et al., 2020, 2022). At the same time, the  
51 availability of surplus moisture at shallow depths minimises the need for ecosystems to invest in extensive  
52 (deeper and lateral) root systems (Bruno et al., 2006). Furthermore, forest ecosystems adapt to climate change by  
53 optimising water distribution through mechanisms such as hydraulic redistribution (Liu et al., 2020; Oliveira et  
54 al., 2005), enhancing water-use efficiency by regulating stomatal conductance, and even ~~shedding~~ shedding leaves (Wolfe  
55 et al., 2016) to minimise moisture loss (Barros et al., 2019; Brum et al., 2019; Lammertsma et al., 2011). Despite  
56 their critical role, the dynamic influence of climate change on vegetation's rooting structure and subsoil moisture  
57 is challenging to measure at the ecosystem scale (Fan et al., 2017). Thus, understanding how moisture from wet  
58 periods is stored, transmitted, and lost from ~~the soil, and as well as~~ how it is accessed by vegetation during dry  
59 periods, is critical to the ecohydrology and resilience of terrestrial ecosystems under climate change.

60 However, such ecohydrological dynamics remain challenging to incorporate in Earth System Models  
61 (ESMs) (Lenton, 2011; Maslin and Austin, 2012; Valdes, 2011) – complex mathematical representations of Earth  
62 system processes and interactions across different biospheres. This limits ~~the ESM's~~ capacity ~~of ESMs~~ to simulate  
63 tipping points as an emergent property of the system (i.e., properties that emerge due to multiple interactions  
64 between several system components, and are not the property of an individual component) (Hirota et al., 2021;  
65 Reyer et al., 2015; Singh et al., 2023). This constraint is mainly due to our poor understanding of complex  
66 mechanisms governing the ecosystem, which are not well represented in ESMs. This includes a limited  
67 understanding of vegetation-climate feedbacks (Boulton et al., 2013, 2017; Chai et al., 2021), subsoil moisture  
68 availability (Cheng et al., 2017), ~~ecosystem~~ adaptation dynamics (Yuan et al., 2022), the response time of forest  
69 ecosystems to climate change perturbations, and assumptions about future (i.e., prescribed) land-use change  
70 (Hurttt et al., 2020) in the ESMs. Furthermore, in the Earth system, some interactions still remain largely  
71 unknown, thereby making the prediction of (abrupt) forest-to-savanna transition (referring to changes in the

72 dense-canopy structure of forests to one that mimics an open-canopy structure similar to savanna; hereafter  
73 referred to as forest-savanna transition) challenging (Drijfhout et al., 2015; Hall et al., 2019; Koch et al., 2021).

74 To understand the extent of rainforest tipping risks, there is a need to assess and contrast the forest  
75 resilience consequences of low-emission and current commitment trajectories with the more commonly used  
76 high-emission scenario (Jehn et al., 2022). However, the risk of forest-savanna transitions under various possible  
77 climate future scenarios is relatively under-investigated. As a result of the conflicting findings and scenario-  
78 dependent uncertainties, the Intergovernmental Panel on Climate Change (IPCC) has only low confidence about  
79 the possible tipping of the Amazon forest by the end of the 21<sup>st</sup> century (Canadell et al., 2021). However, with  
80 mounting empirical evidence on how climate change influences rainforest ecosystems (Boulton et al., 2022;  
81 Küçük et al., 2022; Singh et al., 2020, 2022), the research on rainforest resilience loss has accelerated  
82 considerably in the recent decade (Ahlström et al., 2017; Huntingford et al., 2013). Yet, forest resilience is often  
83 assessed based on changes in forest carbon stocks (Huntingford et al., 2013; Parry et al., 2022) or precipitation  
84 (Hirota et al., 2011; Staal et al., 2020; Zemp et al., 2017); and rarely on the subsoil moisture availability of the  
85 ecosystem (Singh et al., 2022).

86 This study aims to assess the state of rainforests and the risk of a forest-savanna transition under the end  
87 of the 21<sup>st</sup>-century climate based on an empirical understanding of ecosystems' root zone storage dynamics. For  
88 this, we use mass-balance derived root zone storage capacity ( $S_r$ ) – representing the maximum amount of soil  
89 moisture vegetation can access for transpiration (Gao et al., 2014; Singh et al., 2020; Wang-Erlandsson et al.,  
90 2016). Our use of  $S_r$  is grounded in its effectiveness in representing ecosystems' access to soil moisture and their  
91 ability to modify above-ground structures accordingly (de Boer-Euser et al., 2016; Singh et al., 2020; Stocker et  
92 al., 2023; Wang-Erlandsson et al., 2016). It should be noted that we refer to rainforest tipping as a forest-savanna  
93 transition 'risk' since the timing of such transitions depends on the stochastic fluctuations of other environmental  
94 factors, beyond just hydroclimate (e.g., fire, human influence, species composition) (Cole et al., 2014; Cooper et  
95 al., 2020; Higgins and Scheiter, 2012; Poorter et al., 2016). Therefore, to project if an ecosystem is a forest or  
96 has tipped to savanna in the future, we assume the hydroclimate projected by the end of the 21<sup>st</sup> century (i.e.,  
97 2086-2100) and ecosystem are in equilibrium. However, we do not account for the time required for ecosystems  
98 to reach their (long-term) equilibrium state, which previous studies suggest can take between 50-200 years after  
99 crossing the tipping point (Armstrong McKay et al., 2022).

100

## 101 **2 Methodology**

### 102 **2.1 Study Area**

103 This study focuses on forest ecosystems (i.e., excluding savanna/grassland and vegetation in human-influenced  
104 ecosystems) extending between 15°N–35°S for South America and Africa.

105

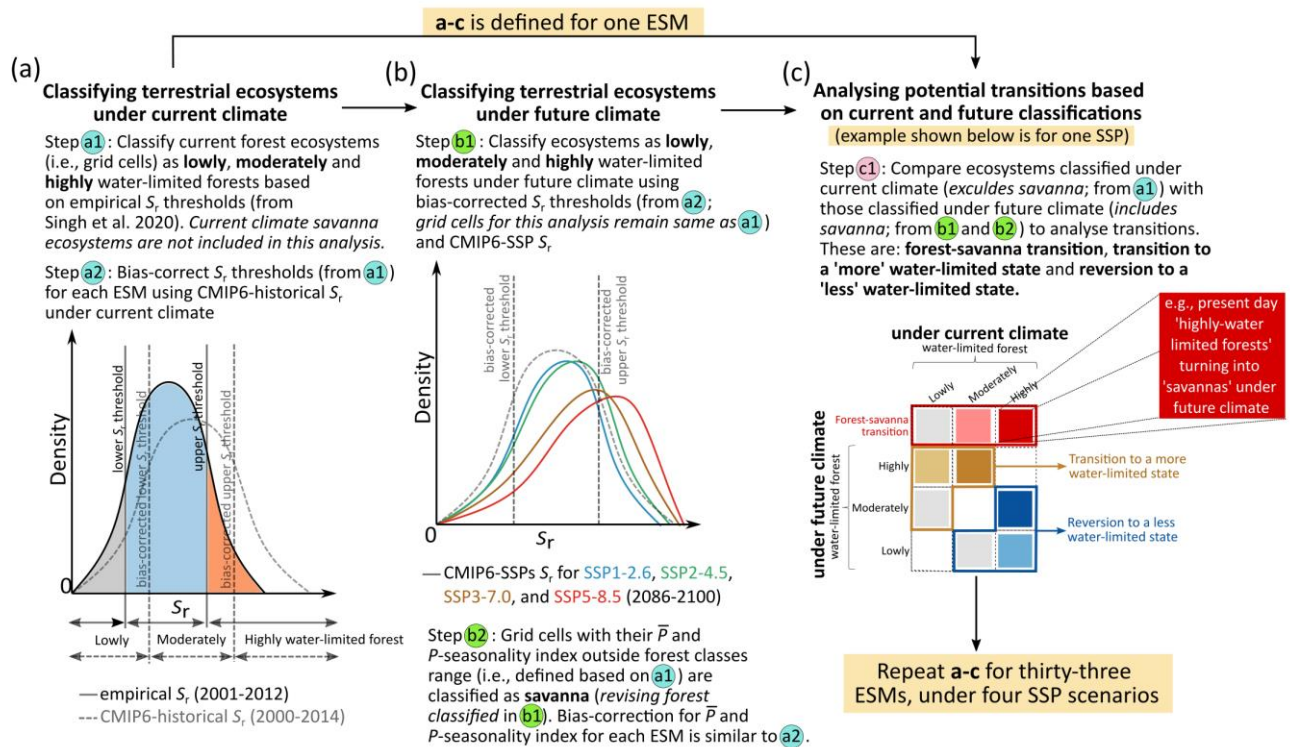
### 106 **2.2 Data**

107 This analysis uses both empirical and ESM-simulated datasets of precipitation and evaporation. Empirical  
108 datasets include remotely sensed and observation-corrected precipitation and evaporation time-series. Empirical  
109 precipitation estimates at daily timestep are obtained from the Climate Hazards Group InfraRed Precipitation  
110 with Station data (CHIRPS; 0.25° resolution) (Funk et al., 2015). Furthermore, empirical evaporation is derived  
111 using an equally-weighted ensemble of three different datasets – (i) Breathing Earth System Simulator (BESS;  
112 0.5° resolution) (Jiang and Ryu, 2016) (ii) Penman-Monteith-Leuning (PML; 0.5° resolution) (Zhang et al., 2016)  
113 and (iii) FLUXCOM-RS (0.083° resolution) (Jung et al., 2019) - at monthly timestep. Here, evaporation  
114 represents the sum of all evaporated moisture from the soil, open water and vegetation, including interception  
115 and transpiration. We only selected evaporation datasets free from biome-dependent parameterisation (such as  
116 plant function types, stomatal conductance, and maximum root allocation depth) and soil layer depth (represents  
117 maximum depth of moisture uptake). Ultimately, all evaporation datasets are bilinearly interpolated to 0.25°  
118 resolution and downscaled to daily timestep using ERA5 evaporation (0.25° resolution) estimates (Hersbach et  
119 al., 2020). All empirical datasets are obtained for 2001-2012.

120 We also obtained precipitation and evaporation estimates from 33 ESMs (from 22 different institutes),  
121 which includes CMIP6-historical and four SSP scenario simulations (SSP1-2.6 leads to approx. 1.3-2.4°C  
122 warming; SSP2-4.5 corresponds to 2.1-3.5°C warming and is closest to the current trajectory according to the  
123 nationally determined contributions (Anon, 2015); SSP3-7.0 around 2.8-4.6°C warming; and SSP5-8.5 represents  
124 3.3-5.7°C warming; °C warming represents an increase in mean global surface temperature change by the end of  
125 21<sup>st</sup> century relative to 1850-1900 (IPCC, 2021) (Fig. 1; Table S1 and S2). The historical estimates are obtained  
126 at a monthly timestep for 2000-2014, and the estimates under different SSPs are obtained for 2086-2100. Though  
127 obtained estimates from different ESMs are at different spatial resolutions, we bilinearly interpolated them to  
128 0.25° for this analysis.

129 Finally, to minimise the influence of human activity and non-forest land cover on the natural water cycle,  
130 we utilised land-cover data to remove pixels with such features from our analysis. We began by removing human-  
131 influenced and non-forest land cover, such as savanna, grasslands, and water bodies, from Globcover, a global  
132 land-cover classification dataset by the European Space Agency (ESA) at 300m resolution (GlobCover land-use  
133 map, 2022). We then performed majority interpolation to convert the dataset to a 0.25° resolution and to mask  
134 grid cells with less than 50% forest cover. This step ensured that only grid cells with over 50% forest cover were  
135 classified as forests for further analysis.

136



137

138

139

140

141

142

143

144

145

146

147

148

149

150

151

152

153

154

155

156

157

158

159

160

161

162

**Figure 1: Methodological framework for analysing the potential transitions in tropical terrestrial ecosystems using empirical and CMIP6-Earth System Models (ESMs) hydroclimate estimates.** (a) We use root zone storage capacity ( $S_r$ )-based classification thresholds (obtained from Singh et al., 2020) – calculated using empirical precipitation ( $P$ ) and evaporation ( $E$ ) estimates (Fig. S1; see Methodology section and Appendix A1) – to classify terrestrial ecosystems under the current climate. Savanna ecosystems under the current climate are excluded from this analysis. We bias-correct these  $S_r$  thresholds for all ESMs using the histogram equivalence method (Piani et al., 2010) (Table S1). (b) We then use these bias-corrected  $S_r$  thresholds to classify ecosystems under future climate conditions (Fig. S2 and S3). Furthermore, we use mean annual precipitation ( $\bar{P}$ ) and  $P$ -seasonality index range ( $S_r$ -based forest classes from a) - as a proxy for ecosystem state - to revise our classification under future climate (Appendix A3 and Fig. S4). (c) We then analyse the potential transitions by comparing ecosystems classified under the current climate (analysed in a) with those classified under future climate (analysed in b) individually for all ESMs (Fig. S5 and S6). The transition analysis assumes that the ~~vegetation and~~ hydroclimate and the ecosystem are in equilibrium, and does not account for the time required for transitions to occur. A detailed description is provided in the Methodology section. An exemplification of this methodological framework is shown in Fig. S7.

### 2.3 Root zone storage capacity-based framework for projecting forest transitions

Vegetation uptakes soil moisture from its roots; thus, the availability of root zone moisture is a key element that mediates the interaction between vegetation and climate (Brooks et al., 2015; Küçük et al., 2022; Rosas et al., 2019; Wang-Erlandsson et al., 2022). However, measuring soil- (such as texture and porosity) and root-characteristics (such as vertical and lateral extent and soil moisture uptake profiles) that influence access to subsoil moisture are challenging to measure at ecosystem scales (Bruno et al., 2006). Furthermore, land-system models tend to oversimplify the transfer and storage of water in root-zone due to insufficient knowledge about soil-vegetation-climate interactions (Albasha et al., 2015; Hildebrandt et al., 2016; Wang et al., 2004). In such cases, the mass-balance approach-based  $S_r$  provides a tangible and comprehensive understanding of ecosystem

163 access to moisture stored in the soil (de Boer-Euser et al., 2016; Gao et al., 2014; McCormick et al., 2021; Stocker  
164 et al., 2023).

165

### 166 **2.3.1 Estimating mass-balance derived root zone storage capacity ( $S_r$ )**

167 Derived using the mass-balance approach,  $S_r$  represents the maximum amount of soil moisture accessed by  
168 vegetation for transpiration (Singh et al., 2020; Wang-Erlandsson et al., 2016). This methodology calculates the  
169 maximum extent of soil moisture within the reach of plant roots, assuming that ecosystems do not invest in  
170 expanding their root-zone storage beyond what is necessary to bridge the maximum (accumulated) water-deficit  
171 experienced by the vegetation during dry periods (i.e., periods in which evaporation is greater than rainfall,  
172 irrespective of the seasons). This maximum annual accumulated water deficit ( $D_{a,y}$ ) experienced by the ecosystem  
173 is calculated using daily precipitation and evaporation estimates (Appendix A1 and Fig. A1). Subsoil moisture  
174 beyond the reach of plant roots is primarily controlled by gravity-induced gradients (de Boer-Euser et al., 2016)  
175 and is not available for transpiration. The rationale is that any extensive investment (i.e., more than necessary)  
176 in root expansion would require carbon allocation and, thus, is inefficient from the perspective of the plants (Gao  
177 et al., 2014; Schenk, 2008). Since this approach does not rely on prior information about vegetation, soil, or land  
178 cover-based, by using empirical (observation-based) datasets (Appendix A1 and Fig. A1), we capture the  
179 dynamics of actual soil moisture available for the ecosystems (Wang-Erlandsson et al., 2016). The detailed  
180 methodology for calculating  $S_r$  using precipitation and evaporation estimates is outlined in Appendix A1.

181 In this mass-balance approach,  $S_r$  only represents a hydrological buffer essential for maintaining the  
182 ecosystem's structure and functions (Gao et al., 2014; Wang-Erlandsson et al., 2016). However, other biotic and  
183 abiotic factors, such as root morphology, soil depth, and geological formations, can physically restrict  $S_r$  by  
184 limiting rooting depth, rooting structure, and the soil's water-holding capacity (Canadell et al., 1996; Jackson et  
185 al., 1996; Schenk and Jackson, 2002) (Appendix A2). Additionally, soil properties like porosity or field capacity  
186 could necessitate a deeper rooting strategy in different soil types (e.g., between sandy and clayey soil) to achieve  
187 a comparable level of  $S_r$  to sustain the ecosystem under future climate (Kukul and Irmak, 2023). However, this  
188 study assesses the impact of future climate change on the ecosystem's hydrological regime, focusing on the  
189 changes to the ecosystem's equilibrium state. Therefore, the direct influence of soil and root characteristics under  
190 future climate change on  $S_r$  (Appendix A2) and forest transitions falls outside our current scope.

191

### 192 **2.3.2 Determining root zone storage capacity thresholds for forest transitions**

193 A recent study by Singh et al. (2020) demonstrated that  $S_r$  can effectively represents an ecosystem's above-  
194 ground state (i.e., whether it is a forest or savanna) and its level of water-stress, based on root-zone moisture  
195 availability. In this study, we refine their terminology from 'water-stressed state' to 'water-limited state' to more  
196 precisely describe the effects of changes in hydroclimatic conditions on forest and savanna -ecosystems;  
197 ~~specifically in terms of inhibiting plant growth based on subsoil moisture availability and the potential of them~~

198 approaching the threshold of forest-savanna transition. According to Singh et al. (2020), in response to water-  
199 limited conditions, forests adapt their rooting strategies and modify their above-ground forest cover. These  
200 adaptations aim to allocate carbon in the most efficient way possible to maximise the hydrological benefits  
201 available to the ecosystem. They classified these terrestrial ecosystems responses into four distinct categories  
202 based on the relationship between tree cover density and root zone storage capacity ( $S_r$ ); ~~illustrating the various~~  
203 ~~drought-coping strategies of ecosystems~~ (for a more detailed description, ~~see provided in~~ Singh et al., 2020):

- 204 i. **Lowly water-limited forest:** Dense forests (>70% tree cover) that receive ample rainfall (with daily  
205 precipitation exceeding evaporation year-round; Singh et al., 2020) results in a very low  $D_{a,y}$  (Appendix  
206 A1). In such an environment, the top layer of the soil remains consistently damp, allowing for efficient  
207 soil moisture uptake through shallow roots (<1m;  $S_r$  and maximum rooting depth comparison in Singh et  
208 al., 2020), as vegetation typically utilises the shortest available pathway for moisture uptake (Bruno et  
209 al., 2006). Consequently, these forest ecosystems can sustain themselves with a low  $S_r$  (<100 mm) (Singh  
210 et al., 2020).
- 211 ii. **Moderately water-limited forest:** Although these forests retain a dense structure (>65% tree cover), the  
212 increased precipitation seasonality (evaporation rates remain the same as before; ~~(Singh et al., 2020)~~)  
213 leads to a relatively higher  $D_{a,y}$  (Appendix A1). This necessitates a greater investment in their rooting  
214 systems to access subsoil moisture for dry periods, with  $S_r$  for these ecosystems ranging between 100-  
215 400 mm in South America and 100-350 mm in Africa (Singh et al., 2020). Notably, this enhanced below-  
216 ground investment does not compromise the above-ground ecosystem structure, as evidenced by the  
217 changes in ecosystem rooting structure relative to tree cover (Singh et al., 2020).
- 218 iii. **Highly water-limited forest:** With further increase in precipitation seasonality (even negligible  
219 precipitation during dry seasons) and duration of dry period, forests need to maximize their  $S_r$   $S_r$  to sustain  
220 their structure (see Fig. S2 and S3 in Singh et al., 2020). ~~(maximum~~ Maximum rooting depths of these  
221 ecosystems can typically range between 15-20m (Singh et al., 2020). Maintaining ecosystems under  
222 these conditions is costly from a subsoil investment perspective (Schenk, 2008), with regions in South  
223 America and Africa showing  $S_r$  values as high as 750 mm and 450 mm, respectively (Singh et al., 2020).  
224 Consequently, these values represent the upper limits beyond which forest ecosystems cannot further  
225 enhance their  $S_r$  (Singh et al., 2020).

226 Possible mechanisms suggest that these trees adapt by shedding leaves to minimise moisture loss  
227 (Wolfe et al., 2016). However, this adaptation can reduce photosynthetic activity, leading to declines in  
228 root growth, and heightening the risk of mortality from hydraulic failures due to the unavailability of soil  
229 moisture at accessible depths (Guswa, 2008). Furthermore, the accumulation of dry leaves also  
230 perpetuates forest fires, thinning the ecosystem even further (tree cover can drop as low as 30%) (Nepstad  
231 et al., 1999; Singh et al., 2020). Although increased tree mortality reduces competition for water, enabling  
232 some trees to survive, the heightened risk of hydraulic failures and forest fires makes these ecosystems  
233 highly susceptible to transitioning to savanna (Anderegg et al., 2016; Oliveras and Malhi, 2016; Sperry  
234 and Love, 2015).

235 iv. **Savanna-grassland regime** (hereafter referred to as **savanna**): These ecosystems, typically  
236 characterised by an open, grass-dominated structure (tree cover <40%), have both a lower water  
237 availability and demand (both precipitation and evaporation are lower than in forest ecosystems) (Ratnam  
238 et al., 2011; Singh et al., 2020). Thus, requiring a lower hydrological buffer to sustain their structure and  
239 functions. For these ecosystems,  $S_r$  values can be as low as 100 mm (Singh et al., 2020). Although tree  
240 species in this ecosystem can develop deep roots (extending up to 20m; see Fig. 2 and 3 in Singh et al.,  
241 2020), the majority of the root biomass is concentrated in the shallow soil layers (top 30–50 cm; shallow  
242 water uptake profile) (February and Higgins, 2010; Schenk, 2008). This strategy allows for **completive**  
243 **competitive** moisture uptake between trees and grass species (Nippert and Holdo, 2015). This also  
244 suggests that, for savanna, deeper roots don't always necessitate a high  $S_r$  (Singh et al., 2020).  
245

246 The difference in  $S_r$  thresholds between both continents is due to the presence of water-use-efficient C4  
247 grasses in Africa (Still et al., 2003), which reduces the competitiveness for moisture uptake between tree species  
248 and grasses – leading to a lesser need for extensive  $S_r$  in the African forest ecosystem (Singh et al., 2020).  
249 Furthermore, these adaptation dynamics align with the alternative stable state theory (i.e., forest's stabilising  
250 feedback under hydroclimatic changes and tipping risk beyond certain hydroclimatic extremes) (Hirota et al.,  
251 2011), which makes  $S_r$  more representative of the transient state of the ecosystem than precipitation (Singh et al.,  
252 2022). We, thus, use these mass-balance derived  $S_r$  thresholds to project rainforest transitions and tipping risk  
253 under future climate change. A detailed description of how previous studies have projected rainforest tipping  
254 (Table S3), and how  $S_r$ -based framework builds upon their shortcomings is mentioned in the Supplement.  
255

### 256 2.3.3 Projecting forest transitions under future climate change

257 ~~To project forest transitions under future climate, we have to first classify forests based on  $S_r$  thresholds~~  
258 ~~under the current and future climate. Based on this classification, we analyse potential transition for each ESM~~  
259 ~~and aggregate the results (Fig. 1). Due to the lack of appropriate metrics for vegetation structure (e.g., tree cover~~  
260 ~~density, tree height, floristic patterns) and the reliance on assumptions about future land-use change (i.e.,~~  
261 ~~prescribed rather than biophysically simulated) in ESMs (Hurt et al., 2020), we use hydroclimate from ESMs as~~  
262 ~~a proxy to project forest transitions under future climate conditions. Using this proxy, we assume that the~~  
263 ~~hydroclimate projected for the end of the 21<sup>st</sup> century and the ecosystem are in equilibrium~~ (Staal et al., 2020).  
264 We start by classifying forests under the current climate following the approach by Singh et al. (2020), which  
265 uses the (empirical) daily estimates of CHIRPS precipitation and ensemble evaporation (2001-2012) (Appendix  
266 A1 and Sect. 2.3.2) (Fig. 1a). Since we are only interested in forest transitions, the ecosystems classified as  
267 savanna under the current climate are excluded from this analysis.

268 Next, for classifying ecosystems under future climate scenarios (Fig. 1b), we follow the same mass-balance  
269 approach (Appendix A1). However, since precipitation and evaporation estimates from ESMs do not align with  
270 empirical estimates (Baker et al., 2021; McFarlane, 2011), we employ a bias-correction method. Specifically, we



271 use a histogram equivalence method (Piani et al., 2010) to adjust empirical  $S_r$  thresholds to comparable CMIP6  
272  $S_r$  thresholds for various ESMs (Table S1). This involves, first, calculating  $S_r$  using CMIP6-historical  
273 precipitation and evaporation estimates between 2000-2014 (Appendix A1 and Fig. S8). We then determine  
274 percentile-equivalent  $S_r$  thresholds for each of the thirty-three CMIP6-ESMs under the current climate. For  
275 example, if an empirical  $S_r$  of 100 mm corresponds to the 10<sup>th</sup> percentile ( $n = 20\%$  of total pixels), we find the  
276 10<sup>th</sup> percentile in the CMIP6-historically  $S_r$ , which may be higher or lower than 100 mm for each ESM (Fig. 1  
277 and Table S1). These percentile-equivalent  $S_r$  thresholds are then used to classify ecosystems both under current  
278 (CMIP6-historical; 2000-2014) and future climate (CMIP6-SSPs; 2086-2100) (Fig. 1b). Classifying savanna  
279 under future climate requires an additional step as outlined in Appendix A3.

280 Ultimately, we evaluate potential transitions by comparing ecosystems classified under current climate  
281 conditions (*this excludes savanna*) with those under future climate conditions (*this includes savanna*) (Sect.  
282 2.3.2). These transitions are divided into three distinct categories (Fig. 1c and Fig. A2):

- 283 i. **Forest-savanna transition:** This refers to current climate forest ecosystems that risk transitioning to a  
284 savanna under future climate change.
- 285 ii. **Transition to a more water-limited state:** This includes ecosystems that shift to a higher water-limited  
286 state in the future. For example, if a forest currently classified as lowly water-limited transitions to either  
287 a moderately or highly water-limited state in the future, it would fall under this category.
- 288 iii. **Reversion to a less water-limited state:** This includes ecosystems that shift to a lower water-limited  
289 state in the future.

290  
291 To aggregate the results from all ESMs, grid cells with  $> 50\%$  convergence are referred to as ‘moderate-  
292 high model agreement’, 20-50% as ‘moderate model agreement’ and  $\leq 20\%$  as ‘low model agreement’. In the  
293 Results section, we primarily discuss estimates from scenarios  $>20\%$  and  $>50\%$  model convergence. While a  
294 threshold of  $>20\%$  may seem low given the total number of ESMs analysed, it is important to recognise the  
295 variable and often limited capabilities of these ESMs, particularly in simulating biophysical interaction and  
296 emerging properties due to our limited understanding of the Earth system (Lenton et al., 2019; Stevens and Bony,  
297 2013). Opting for a majority-based consensus in ESMs could overlook critical tipping risks identified by a  
298 minority of models, which might provide insights as valid as those from more widely agreeing models (Arora et  
299 al., 2023; Reyer et al., 2015).

300

## 301 2.4 Sensitivity analyses

302 Our methodology operates under two key assumptions: (i) the empirically derived  $S_r$  thresholds remain valid in  
303 the future, and (ii) the hydroclimatic estimates projected by ESMs accurately represent the actual climate, even  
304 though these models have prescribed land-cover (Hurtt et al., 2020). To address the uncertainties related to the  
305 first assumption, we conduct four sensitivity analyses to assess the robustness of our analysis: (a) assuming that  
306 the regions exceeding the 99<sup>th</sup> percentile  $S_r$  are prone to a forest-savanna transition, as high  $S_r$  investment could

307 be unrealistic from the perspective of plants under future climate change, (b) evaluating forest transitions using  
308 three different evaporation datasets, (c) assessing forest transitions under 10- and 40-year drought return periods,  
309 and (d) adjusting the forest-savanna transition thresholds.

310 Regarding the second assumption, we explicitly apply this methodology across a wide range of available  
311 ESMs under four SSP scenarios to identify consistencies and discrepancies in the results. Additionally, the  
312 discrepancies between the prescribed land-use and the forest transitions derived from our methodology, as well  
313 as the implications of these assumptions, are detailed in the Discussion section.

314

### 315 **3 Results**

316 We find that under future climate conditions (2086-2100), considering >50% models' agreement, about one-  
317 fourth of the forests in both South America and Africa are projected to transition (Fig. 2b-g). With >20% models'  
318 agreement, these transitions are projected to occur for about three-fourths of the forests for both continents.  
319 Considering a lower threshold for models' agreement causes double or triple counting of some transitions (Fig.  
320 2b-g). To minimise this in further analyses, we only consider >50% models' agreement for forests that transition  
321 to a more and less water-limited state. Furthermore, because (abrupt) forest-savanna transitions are under-  
322 represented in ESMs (Drijfhout et al., 2015; Lenton, 2011; Maslin and Austin, 2012; Valdes, 2011), we consider  
323 >20% models' agreement for them. Considering this, we not only reduce the overlap to <0.4% of the total forest  
324 area (Fig. S9), but we also maximise highlighting forest-savanna transition risk for both continents.

325 We find that the risk of forest-savanna transitions mainly occurs in the Guiana Shield of South America,  
326 and the southern and south-eastern regions of Africa (Fig. 3). Compared to Africa, forest-savanna transitions are  
327 more prominent in South America under warmer climates (i.e., higher SSPs; Fig. 2b and 3). Our analysis reveals  
328 that the extent of forest-savanna transitions in South America decreases from almost  $1.32 \times 10^6 \text{ km}^2$  (16.3% of  
329 total forest area in South America) under the highest emission scenario to  $0.04 \times 10^6 \text{ km}^2$  (0.5%) under the lowest  
330 emission scenario (Fig. 2b). Interestingly, for Africa, the extent of forest-savanna transition did not change much  
331 for different SSPs, i.e., (median)  $0.25 \times 10^6 \text{ km}^2$  with a maximum deviation of  $\pm 0.11 \times 10^6 \text{ km}^2$  (minimum and  
332 maximum extent of transition between 3-6.6% of total forest area in Africa) (Fig. 2c).

333 When comparing the changes in forest-savanna transition risk areas relative to their immediate lower  
334 warming scenarios, we find considerable increases for South America. The highest relative growth of  
335 approximately 5.75 times is observed between SSP1 and SSP2, with the forest area under risk increasing from  
336  $0.04 \times 10^6 \text{ km}^2$  to  $0.23 \times 10^6 \text{ km}^2$ , respectively. It increases by 3.48 times from SSP2 to SSP3 ( $0.23 \times 10^6 \text{ km}^2$  to  
337  $0.80 \times 10^6 \text{ km}^2$ ), and by 1.65 times from SSP3 to SSP5 ( $0.80 \times 10^6 \text{ km}^2$  to  $1.32 \times 10^6 \text{ km}^2$ ). For Africa, however,  
338 the increases are more modest: the risk grows by 1.29 times from SSP1 to SSP2 ( $0.17 \times 10^6 \text{ km}^2$  to  $0.22 \times 10^6$   
339  $\text{km}^2$ ), by 1.63 times from SSP2 to SSP3 ( $0.22 \times 10^6 \text{ km}^2$  to  $0.36 \times 10^6 \text{ km}^2$ ), and is observed to decrease by 0.72  
340 times from SSP3 to SSP5 ( $0.36 \times 10^6 \text{ km}^2$  to  $0.26 \times 10^6 \text{ km}^2$ ).

341 By evaluating changes to their hydroclimate, we find that under warmer climates, forest-savanna transition  
342 regions in both continents are projected to experience a decrease in precipitation. Furthermore, we observe an

343 increase in precipitation seasonality for South America, whereas Africa shows a decrease (Fig. S12). Here, an  
344 increase in precipitation seasonality (seasonal variability in precipitation over the year) creates water-limited  
345 conditions for the ecosystem. In contrast, a decrease in seasonality and precipitation in Africa corresponds to a  
346 lower moisture availability altogether. Nevertheless, for both these continents, this transition seems to occur for  
347 the previously highly water-limited forests under the current climate, followed by moderately, with the least  
348 contribution from lowly water-limited forests (Fig. 3). This highlights the looming risk on highly water-limited  
349 forests to experience a forest-savanna transition under warmer climates.

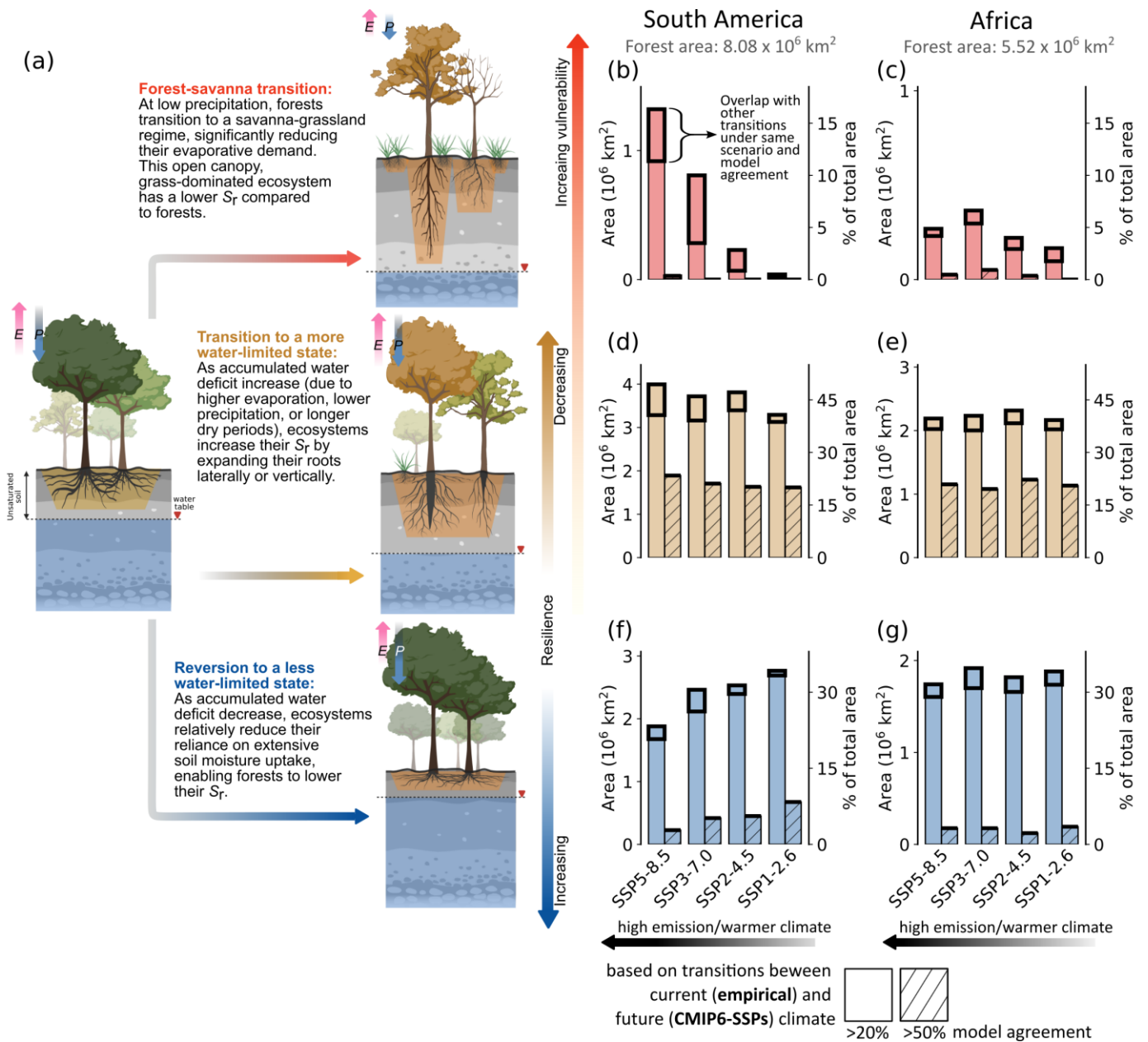
350         Forests that transition to a ‘more’ water-limited state in South America are spatially aggregated towards  
351 the border between Brazil, Colombia, and Peru – covering a considerable portion of the Central Amazon (Fig.  
352 3). Whereas for Africa, these forests exist in moderate to small patches towards the northern and southern extent  
353 of central Congo rainforests. We observe that these transitions account for most of the projected changes to  
354 forests’ states across both continents (Fig. 2d,e), with the transition to just the ‘highly water-limited forest’  
355 accounting for more than three-fourths of all such transitions (Fig. 3). We observe that South American forests  
356 gradually become increasingly water-limited under warmer climates, with maximum and minimum projected  
357 transition of  $1.89 \times 10^6 \text{ km}^2$  (23.4%) and  $1.61 \times 10^6 \text{ km}^2$  (19.9%) observed under the highest and lowest emission  
358 scenarios, respectively (Fig. 2d,e). Whereas for Africa, the change in the water-limited state of the forests under  
359 different SSP scenarios remains almost similar (i.e., median  $1.14 (\pm 0.06) \times 10^6 \text{ km}^2$ ; 19.6-22.2%). Analysis of  
360 their hydroclimatic changes reveals that water-limitation is induced by both a decrease in precipitation and an  
361 increase in seasonality in South America (Fig. S13). In contrast, water-limitation in Africa is driven solely by an  
362 increase in seasonality. We observe that these newly water-limited forests seem to have permeated to regions that  
363 were previously (under the current climate) dominated by lowly and moderately water-limited forests (Fig. 3).  
364 Here, this shift only signifies the changes to hydroclimatic conditions allowing forests to transition to a more  
365 water-limited state, rather than the changes to the floristic composition of terrestrial species from one location to  
366 another. Although such a shift under changing climate is not unlikely (Esquivel-Muelbert et al., 2019), they are  
367 not analysed in this study.

368         Forests that revert to a ‘less’ water-limited state in South America are primarily observed in the south-  
369 eastern Amazon, with small patches observed towards eastern Brazil and the western coast of Equatorial Guinea  
370 and Gabon (Fig. 3). For Africa, the reverted forests exist in patches in the northern and southern regions of the  
371 Congo rainforest. Furthermore, for South America, we observe a gradual decrease in these reversions with an  
372 increase in warming. Here, we observe the lowest reversion of  $0.23 \times 10^6 \text{ km}^2$  (2.8%) under the highest emission  
373 scenario and the highest reversion of  $0.67 \times 10^6 \text{ km}^2$  (8.4%) under the lowest emission scenario (Fig. 2f,g). For  
374 Africa, these trends remain almost similar under all SSPs (i.e., median  $0.18 (\pm 0.05) \times 10^6 \text{ km}^2$ ; 2.2-3.5%).  
375 Comparing these transitions with their hydroclimatic changes reveals an overall increase in precipitation (Fig.  
376 S14). Interestingly, we observe a much higher precipitation increase for South America under high-emission  
377 scenarios than those in lower-emission scenarios. However, we find that precipitation seasonality is also higher  
378 for these ecosystems under warmer climates (Fig. S14). This suggests that increased precipitation without

379 changes to precipitation seasonality helps decrease the water-limitation of the ecosystem, compared to the  
 380 ecosystems that experienced a simultaneous increase in both.

381 Our sensitivity analysis, detailed in Appendix B1, reveals a consistent pattern of forest transitions across  
 382 various scenarios.

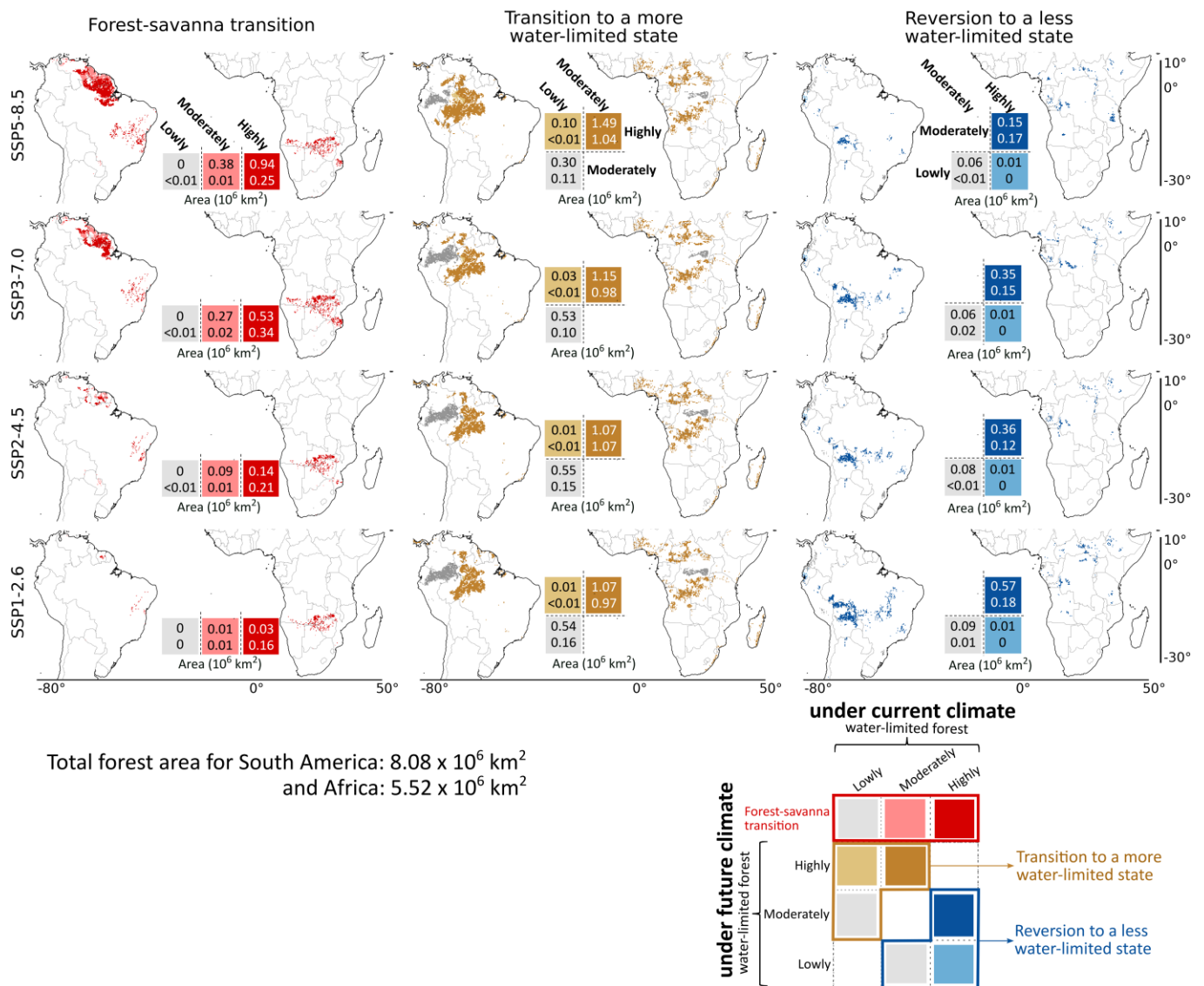
383  
 384  
 385  
 386  
 387



388 **Figure 2: Comparing the potential transitions under different SSP scenarios.** (a) The state of the ecosystem,  
 389 both above- and below-ground, (post-transition) under future climate, quantifying (b,c) forest-savanna transition,  
 390 (d,e) forests' that transition to a more water-limited state and (f,g) revert to a less water-limited state for South  
 391

392 America and Africa (present forest area mentioned on the top of (b,c)), respectively. For the analysis above,  
 393 transitions are calculated for grid cells with model agreement >20% (plain bar plot) and >50% (hatched bar plot).  
 394 These quantifications show changes in the forest area based on ecosystem transitions under empirical-current  
 395 (2001-2012) and future (2086-2100) climate conditions. For all these transitions, we assume that the hydroclimate  
 396 and the vegetation ecosystem are in equilibrium. Analyses comparing ecosystem transitions based on CMIP6-  
 397 historical (2000-2014) and future (2086-2100) climate conditions are shown in Fig. S10 and S11. For each  
 398 transition, the total area of spatial overlap with other transitions under the same SSP scenario and model  
 399 agreement is highlighted with thick black bars. The *P* and *E* arrows in (a) describe the relative magnitude of  
 400 precipitation and evaporation fluxes. The illustration in (a) is adapted from Singh et al. (2020) and created with  
 401 [BioRender.com](https://www.biorender.com).

402



403

404 **Figure 3: Spatial extent of potential transitions with respect to their current state under different SSP**  
 405 **scenarios.** We analysed transitions, explicitly focusing on forest-savanna transition, transition to a more water-  
 406 limited state, and reversion to a less water-limited state, by comparing different ecosystem classes under current  
 407 (empirical; 2001-2012) and future (SSPs; 2086-2100) climate conditions (as defined in Fig. 2). All transitions  
 408 shown above are analysed for moderate-high (>50%) model agreement, except forest-savanna transition, for  
 409 which moderate (>20%) model agreement is considered. Values overlaying the legends correspond to the total  
 410 area of transition for South America (top values) and Africa (bottom values).

411

## 412 **4 Discussion**

### 413 **4.1 Asynchronous resilience risks under future climate change**

414 Our analysis reveals the spatial extent of potential ecosystem transitions in South America and Africa and their  
415 vulnerability to future climate change (Fig. 2 and 4). For South America, we find a clear indication of a decrease  
416 in forest resilience (i.e., an increase in water-limited forests) and an increase in forest-savanna transition risk  
417 under warmer climates (Fig. 2b,d,f). In contrast, these trends are not symmetric for Africa, where transition risk  
418 shows only slight variation across the different SSPs (Fig. 2c,e,g). Similar to the results of this study, previous  
419 studies on rainforest tipping have also suggested that exceeding 1.5-2°C will considerably increase the tipping  
420 risk (Flores et al., 2024; Jones et al., 2009; Parry et al., 2022), with the Guyana Shield in the Amazon being the  
421 most susceptible under future climate change (Cox et al., 2004; Staal et al., 2020) (Fig. 3 and Table S3). Previous  
422 studies also agree that, in contrast to the Amazon, the projected risk to Congo rainforests is not substantial  
423 (Higgins and Scheiter, 2012; Staal et al., 2020) (Fig. 2). Despite it being unclear to what extent the ESMs  
424 represent the correct carbon-water dynamics (Koch et al., 2021), our results show a further divergence between  
425 Amazon's and Congo's responses to different SSPs (Fig. 2 and Fig. S12-S14). This could either be caused simply  
426 by a different response to changes in precipitation patterns over the respective regions (Kooperman et al., 2018;  
427 Li et al., 2022) or a different response to increased CO<sub>2</sub> levels in the atmosphere (Brienen et al., 2015; Hubau et  
428 al., 2020; Trumbore et al., 2015).

429 Previous empirical studies have linked these divergent responses to evolutionary and biogeographical  
430 differences between the ecosystems, which resulted in distinct species pools that uniquely influence each  
431 ecosystem's adaptability and response to climate change (Fleischer et al., 2019; Hahm et al., 2019; Hubau et al.,  
432 2020; Slik et al., 2018). These studies found that forest ecosystems in the Amazon tend to be more dynamic –  
433 grow faster due to high CO<sub>2</sub> levels in the atmosphere – than those in the Congo rainforests. However, these fast-  
434 growing trees also die young due to them investing substantially less in their adaptive strategies against  
435 perturbations than (less dynamic) old-growth forests (Brienen et al., 2015; Körner, 2017; Rammig, 2020). This  
436 makes the Amazon rainforest especially sensitive to CO<sub>2</sub> emissions pathways, as the positive influence of CO<sub>2</sub>  
437 fertilisation-induced growth is counteracted by the negative impact of warming and droughts, thereby  
438 exacerbating the risk of forest mortality under high emission scenarios (Brienen et al., 2015; Hubau et al., 2020;  
439 Yang et al., 2018). In this case, the projected changes to the future hydroclimate could be an artefact of decreased  
440 transpiration and precipitation due to forest mortality, rendering the rainforests vulnerable to tipping. In contrast,  
441 terrestrial species in Congo rainforests appear more resilient, having adapted to severe droughts during glacial  
442 periods, which makes them better equipped to handle episodic water-induced perturbations than Amazon (Cole  
443 et al., 2014).

444 Nevertheless, with compounding influence from land-use and climate-induced hydroclimatic changes  
445 (Davidson et al., 2012), these rainforests risk tipping to a savanna state. Our results highlight that by keeping the  
446 mean global surface temperature below 1.5-2°C warming (which in this case is equivalent to SSP1-2.6 relative

447 to the pre-industrial), we minimise forest-savanna transition risk and maximise recovery – thereby improving the  
448 resilience of rainforest ecosystems (Fig. 2, 3 and 4).

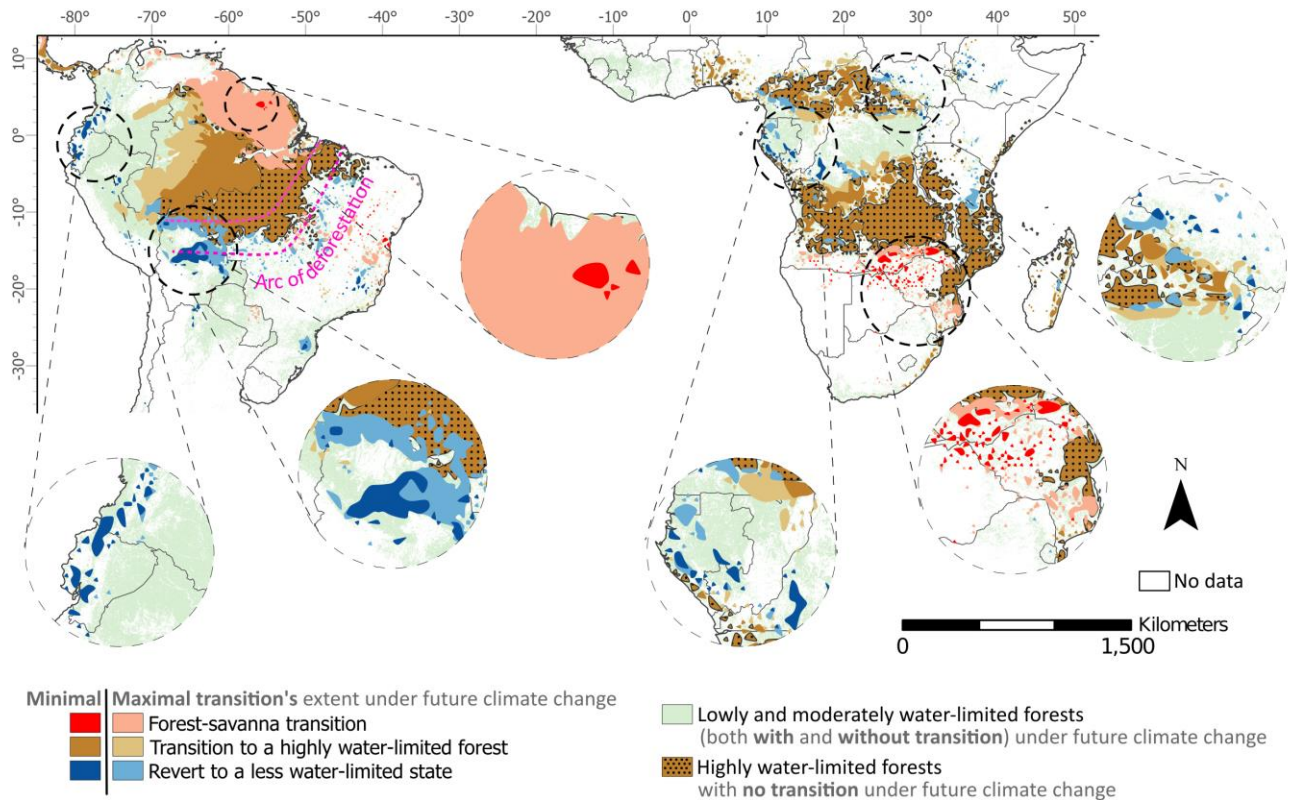
449

#### 450 **4.2 Changes in atmospheric moisture flow drives forest-savanna transition**

451 Among all transitions, the most noticeable and catastrophic (since it is difficult to revert) is the forest-savanna  
452 transition projected in the Amazon’s Guiana Shield of South America, and over the southern and south-eastern  
453 parts of Africa (Fig. 3 and 4). These transitions are associated with the shifting of the inter-tropical convergence  
454 zone (ITCZ) (Mamalakis et al., 2021), which decreases precipitation and increases precipitation seasonality over  
455 the continents. For South America, the creation of these low-pressure bands allows the trade winds to bring in  
456 considerable moisture from the equatorial Atlantic Ocean over to Amazon by passing through the Guiana Shield  
457 and ultimately carrying it across the La Plata Basin via the South American low-level jet (Bovolo et al., 2018;  
458 van der Ent et al., 2010; Zemp et al., 2014). Similarly, for Africa, south-eastern trade winds bring moisture from  
459 the Indian Ocean over the centre of the African continent (Mamalakis et al., 2021).

460 Under a warmer climate, sea surface temperature over the equatorial Atlantic and the northern Indian  
461 Ocean is projected to increase (Pascale et al., 2019; Zilli et al., 2019), leading to a southward shift in ITCZ over  
462 the eastern Pacific and Atlantic Oceans, and northward over east Africa and the Indian Ocean (Mamalakis et al.,  
463 2021; Xie et al., 2010). Previous studies also acknowledge that the intense surface warming over the Sahara under  
464 future climate can also attract ITCZ northwards in Africa (Cook and Vizzy, 2012; Dunning et al., 2018; Mamalakis  
465 et al., 2021). ~~Since~~ These climate change-induced shifts in ITCZ can potentially both mitigate and exacerbate  
466 aggravate (especially critical for highly water-limited forests) the impact-effects of (accumulated) water-deficit  
467 on the forest ecosystem, especially critical for highly water-limited forests, even without considering the changes  
468 including to atmospheric moisture flow caused those caused by localised deforestation (Leite-Filho et al., 2021;  
469 Schumacher et al., 2022; Staal et al., 2018; Wunderling et al., 2022); (Leite-Filho et al., 2021; Schumacher et al.,  
470 2022; Staal et al., 2018; Wunderling et al., 2022). ~~This~~ it warrants underscores the ~~need~~ importance of to  
471 include changes in atmospheric circulation ~~for in~~ studies that analyse ing the impact of future climate on the  
472 resilience of forest ecosystems (Staal et al., 2020; Zemp et al., 2017).

473



474  
 475 **Figure 4: Minimal and maximal extent of potential ecosystem transitions under future climate change in**  
 476 **the entire study region over South America and Africa.** The three transition types are: forest-savanna  
 477 transition, from any class to highly water-limited forests, and to a less water-limited state (see definitions in Fig.  
 478 2 and 3). For better visualisation of these transitions, in this figure, we first converted all grid cells to shape,  
 479 merged them, and then smoothed them using the ‘polynomial approximation with exponential kernel’ function  
 480 (with a tolerance value of 1) in ArcGIS pro. The unsmoothed version of the transitions is shown in Fig. 3. The  
 481 minimal and maximal represent the minimum and maximum possible extent of transitions (as quantified in Fig.  
 482 3) based on changes between current (empirical; 2001-2012) and future (SSPs; 2086-2100) climate conditions  
 483 regardless of the SSP scenarios.

484

### 485 4.3 Discrepancy between prescribed future land-use and projected transitions

486 The land-use information in CMIP6-ESMs is not biophysically simulated, but prescribed based on simulations  
 487 from Integrated Assessment Models (IAMs) for each SSP scenario (Hurt et al., 2020). Therefore, it is valuable  
 488 to examine whether these prescribed land-use scenarios agree or conflict with the changes projected (assuming  
 489 equilibrium between hydroclimate and the ecosystem) by our  $S_r$ -based ecosystem transitions (Fig. 5 and Fig. S15-  
 490 S17).

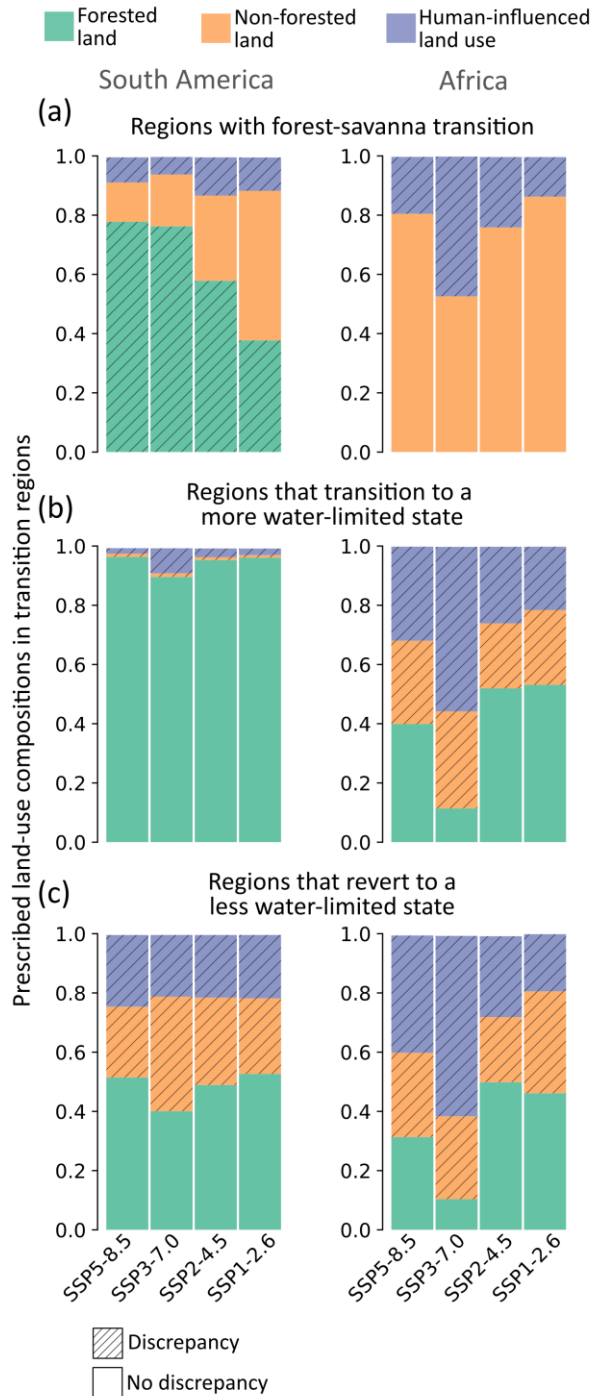
491 The most noticeable discrepancies are observed in South America, where the extent of forest-savanna  
 492 transitions is underestimated in prescribed land-use scenarios compared to those projected in this study (i.e.,  
 493 prescribed land-use predicts forests in the region whose hydroclimate can’t support forest; Fig. 4 and 5a).  
 494 Additionally, in South America, our analysis highlights the potential of some forests reverting to a ‘less water-  
 495 limited state’ in places where the prescribed land-use in the ESMs suggests non-forest landscapes (Fig. 4 and  
 496 5c). These discrepancies arise because the prescribed land-use in CMIP6-ESMs does not shift in response to



497 hydroclimatic changes. Despite our approach assuming equilibrium and overlooking the temporal dynamics of  
498 transitions, based on broad climate change patterns (Sect 4.2), we believe it more accurately represents the  
499 ecohydrological state of the ecosystems.

500 However, these prescribed land-uses can introduce errors in subsequent biophysical processes simulated  
501 in ESMs (Ma et al., 2020), affecting the accuracy of projected transitions. For example, prescribing a region as a  
502 forest that would be grassland in the future will lead to the extraction of deeper subsoil moisture in ESMs, which  
503 (actual) grasslands do not have the capacity to access (Ahlström et al., 2017; Yu et al., 2022). This will result in  
504 an overestimation of the ecosystem's evaporation, potentially altering precipitation patterns downwind and  
505 leading to inaccurate water budget assessments for these ecosystems. Consequently, causing erroneous  
506 projections of the ecosystem state. These discrepancies underscore the urgent need for enhancements in the land  
507 surface components of ESMs, enabling dynamic simulations of vegetation-climate feedbacks. Such  
508 improvements would provide a more accurate representation of the ecohydrology of terrestrial ecosystems and  
509 their response to changing climate conditions.

510



511  
 512 **Figure 5: Prescribed land-use composition for each transition region under different SSP scenarios**  
 513 **(median 2086-2100), calculated as the ratio between the prescribed land use area and the projected**  
 514 **transition area.** Regions where IAM prescribed land use are same as the projected transitions (from Fig. 3)  
 515 are shown in plain colours (i.e., no discrepancy). Whereas regions where IAM-prescribed land use differs from  
 516 projected transitions are hatched (i.e., discrepancy).

517

#### 518 4.4 Limitations

519 This study assumes that the  $S_r$ -derived thresholds used to classify terrestrial ecosystems under current climate  
 520 conditions remain valid under future climate change. However, forests themselves are dynamically adapting their  
 521 structure and functions in response to climate change, altering their critical thresholds (Doughty et al., 2023).

522 Thus, assuming a static critical threshold may lead to inaccuracies in estimating forests' resilience to future  
523 climate change. For instance, under the CO<sub>2</sub> fertilisation effect, forests may become more water-use efficient  
524 (i.e., transpire less and therefore need for a lower  $S_r$ ) (Xue et al., 2015), potentially delaying their tipping under  
525 warming scenarios compared to those projected in this study. Conversely, factors such as nutrient limitation  
526 (Condit et al., 2013) or extensive human influence (van Nes et al., 2016) in the ecosystem might lead to an earlier  
527 tipping than anticipated.

528 However, the uncertainty surrounding the effect of CO<sub>2</sub> fertilisation, nutrient limitation, and human  
529 influence on vegetation remain significant research frontiers for enhancing our understanding of rainforest tipping  
530 under future climate change (Fleischer et al., 2019; Hofhansl et al., 2016). Additionally, factors such as  
531 precipitation variability, species composition, soil properties, and topography can contribute to varied local-scale  
532 forest responses to future climate change (Staal et al., 2020). It should also be noted that though these  
533 uncertainties may hinder our understanding of local-scale forest resilience, the influence of future hydroclimatic  
534 changes on forests still constitutes major prediction uncertainties. Therefore, in this study, regardless of how  
535 these influences are parametrised or simulated in each ESM, we assume that hydroclimatic estimates projected  
536 by the ESMs represent the actual climate.

537 Of course, this assumption opens us and other studies projecting forest conditions to future climate  
538 change to certain limitations. Our ability to project forest-savanna transitions (or any transition) relies on the  
539 model's capacity to simulate complex feedbacks. Some models capture complex vegetation-atmosphere  
540 interaction, simulating local and regional scale feedbacks across time (Ferreira et al., 2011; Jach et al., 2020);  
541 others ~~reply~~ on simpler parametrisation (Nof, 2008) (e.g., parametrisation of CO<sub>2</sub> fertilisation; Koch et al., 2021).  
542 However, caution should be taken to not overgeneralise the functioning of tropical forests just from the analysis  
543 presented in this study, and also realise the current potential of ESMs to simulate them (Staal et al., 2020). We  
544 believe that by considering simulations from multiple ESMs under different SSP scenarios, not only do we  
545 highlight the agreements and conflicts between potential transitions; but also allow future studies to disentangle  
546 vegetation-climate feedbacks and improve the modelling of local-scale interactions (e.g., vegetation's water-  
547 uptake profile, species response to CO<sub>2</sub> fertilisation) in the ESMs.

548

## 549 **5 Conclusions**

550 Classifying terrestrial ecosystems based on empirical and CMIP6 ESMs-derived  $S_r$  allowed us to assess the future  
551 transitions in the rainforest ecosystems. Our findings indicate that the climate projected under the lowest emission  
552 scenarios significantly reduces the risk of rainforest tipping and maximises reversion to a less water-limited state,  
553 while the climate projected under the high emission scenarios ~~have~~-has the opposite effect on the forest  
554 ecosystem. Specifically, in the Amazon rainforest, the risk of forest-to-savanna transition increases considerably  
555 with incremental increases in warming. Conversely, in the Congo, the variation in transition risk across different  
556 emission scenarios is relatively minor.

557 Notably, our analysis suggests a very limited tipping risk that is ‘unavoidable’ (i.e., regions prone to a  
 558 forest-savanna transition in all scenarios), and the vast majority of potential transition risks can still be avoided  
 559 by steering towards a less severe climate scenario, thereby underscoring the critical window of opportunity.  
 560 Moreover, regions projected to revert to a less water-limited state could potentially become more amenable to  
 561 restoration and responsive to deforestation prevention efforts. This study highlights the importance of restricting  
 562 global temperature change below 1.5-2°C warming relative to the pre-industrial levels to prevent forest tipping  
 563 risks and provide the best conditions for effective ecosystem stewardship.

564

## 565 **Appendix A: Methodology**

### 566 **A1. Root zone storage capacity calculation**

567 Our method to calculate  $S_r$  is adopted from Singh et al. (2020). For estimating  $S_r$ , we first obtained the water  
 568 deficit ( $D_t$ ) at daily time step from the daily estimates of precipitation ( $P_t$ ) and evaporation ( $E_t$ ) (Fig. A1) using:

$$569 \quad D_t = E_t - P_t \quad (A1)$$

570 Here,  $t$  denotes the day count since the start of the simulation, with simulation for each grid starting in  
 571 the month with maximum precipitation. Second, we calculated the accumulated water deficit integrated at each  
 572 one-day timestep for one year using:

$$573 \quad D_{a(t+1)} = \max\{0, D_{a(t)} + D_{t+1}\} \quad (A2)$$

574 Where  $D_{a(t+1)}$  is the accumulated water deficit at each time step (Fig. A1). Here, an increase in the  
 575 accumulated water deficit will occur when  $E_t > P_t$ , and a decrease when  $E_t < P_t$ . However, since this algorithm  
 576 estimates a running estimate of root zone storage reservoir size, we use a maximum function to calculate the  
 577 accumulated water deficit, which by definition can never be below zero. Not allowing  $D_{a(t+1)}$  to be negative also  
 578 means that excess moisture from precipitation will either contribute to deep drainage or runoff. Lastly, the  
 579 maximum accumulated annual water deficit ( $D_{a,y}$ ) will represent the maximum storage required by the vegetation  
 580 to respond to the critical dry periods (Fig. A1).

$$581 \quad D_{a,y} = \max\{D_{a(t+1)}\} \quad t = 1 : n - 1 \quad (A3)$$

582 This simulation runs for a whole year, with  $n$  denoting the number of days in year  $y$ .

583 ~~Although different~~ Different terrestrial ecosystems (e.g., forest, savanna and grasslands) adapt to different  
 584 drought return periods (de Boer-Euser et al., 2016; Gao et al., 2014; Wang-Erlandsson et al., 2016). For instance,  
 585 grasslands and savannas adapt to shorter drought return periods (i.e., <10 years and 10-20 years, respectively).  
 586 In contrast, forests adapt to long drought return periods (>40 years) (Wang-Erlandsson et al., 2016). For this  
 587 study, we use a uniform 20-year drought return period (following Bouaziz et al., 2020; Nijzink et al., 2016) to

588 avoid any artificially introduced transitions between different ecosystems. Thus, this 20-year drought return  
 589 period  $S_r$  refers to the maximum amount of root zone moisture accessible to vegetation for transpiration during  
 590 the largest accumulated annual water deficit expected every twenty years under static climate conditions. ~~This~~  
 591 ~~we~~ analyse [this](#) using ~~an~~ the Gumbel extreme value distribution (Gumbel, 1958) and apply it to normalise all

592  $D_{a,y}$ . The Gumbel distribution ( $F(x)$ ) is given by:

$$593 \quad F(x) = \exp \left[ - \exp \left[ - \frac{(x - \mu)}{\alpha} \right] \right] \quad (A4)$$

594 Where  $\mu$  and  $\alpha$  are the location and scale parameters, respectively. We calculate this using the python  
 595 package ‘skextremes’(skextremes Documentation):

$$596 \quad S_r = \overline{D_{a,y}} + K \times \sigma_{n-1} \quad (A5)$$

597 Where  $K$  is the frequency factor given by:

$$598 \quad K = \frac{y_r - y_n}{S_n} \quad (A6)$$

599 And  $y_t$  is the reduced variate given by:

$$600 \quad y_t = - \left[ \ln \left[ \ln \left( \frac{T}{T-1} \right) \right] \right] \quad (A7)$$

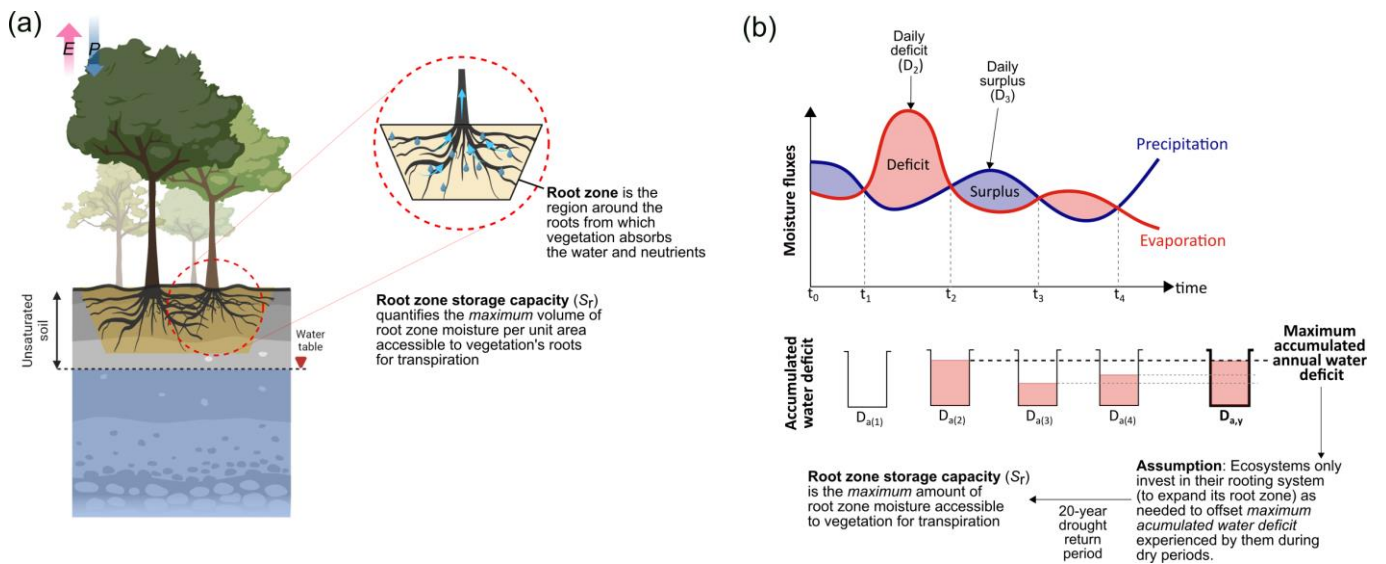
601 Where  $T$  is the drought return period (i.e., 20 years used in this study),  $\overline{D_{a,y}}$  is the mean annual  
 602 accumulated deficit for the years 2001-2012,  $\sigma_{n-1}$  is the standard deviation of the sample. Also,  $y_n$  is the reduced  
 603 mean and  $S_n$  is the reduced standard deviation, which for  $n = 11$  years (since we are calculating  $S_r$  in a hydrological  
 604 year – simulation starts mid-year – we therefore lose one year) is equal to 0.4996 and 0.9676, respectively  
 605 (Gumbel, 1958).

606 Since the CMIP6 (-historical and -SSP estimates, the timeframe considered are 2000-2014 and 2086-  
 607 2100, respectively) doesn’t have daily estimates of evaporation and precipitation for all Earth System Models  
 608 (ESMs), we directly use the monthly estimates of precipitation and evaporation to modify Eq. (A1) as:

$$609 \quad D_t = E_{t(monthly)} - P_{t(monthly)} \quad (A8)$$

610 Here,  $t(monthly)$  denotes the month count since the start of the simulation. The rest of the steps (Eq. A2-  
 611 A7) remain the same for CMIP6 datasets. For CMIP6 runs,  $y_n$  and  $S_n$  in Eq. (6) are calculated for  $n = 14$  years  
 612 (Eq. A7) equal to 0.5100 and 1.0095, respectively. The  $S_r$  estimates derived from daily and monthly empirical  
 613 estimates (from Eq. A1 and A8) are compared in Fig. S8 to evaluate uncertainty.

614



615

616 **Figure A1:** The figure illustrates the root zone storage capacity ( $S_r$ ) of the ecosystem. (a) We show the difference  
 617 between the ecosystem's root zone and how that constitutes its  $S_r$ . (b) Conceptual illustration of how the  
 618 ecosystem's precipitation and evaporation fluxes constitute the maximum accumulated annual water deficit ( $D_{a,y}$ )  
 619 and  $S_r$ . The figure is adopted from Singh (2023) and Wang-Erlandsson et al. (2016).

620

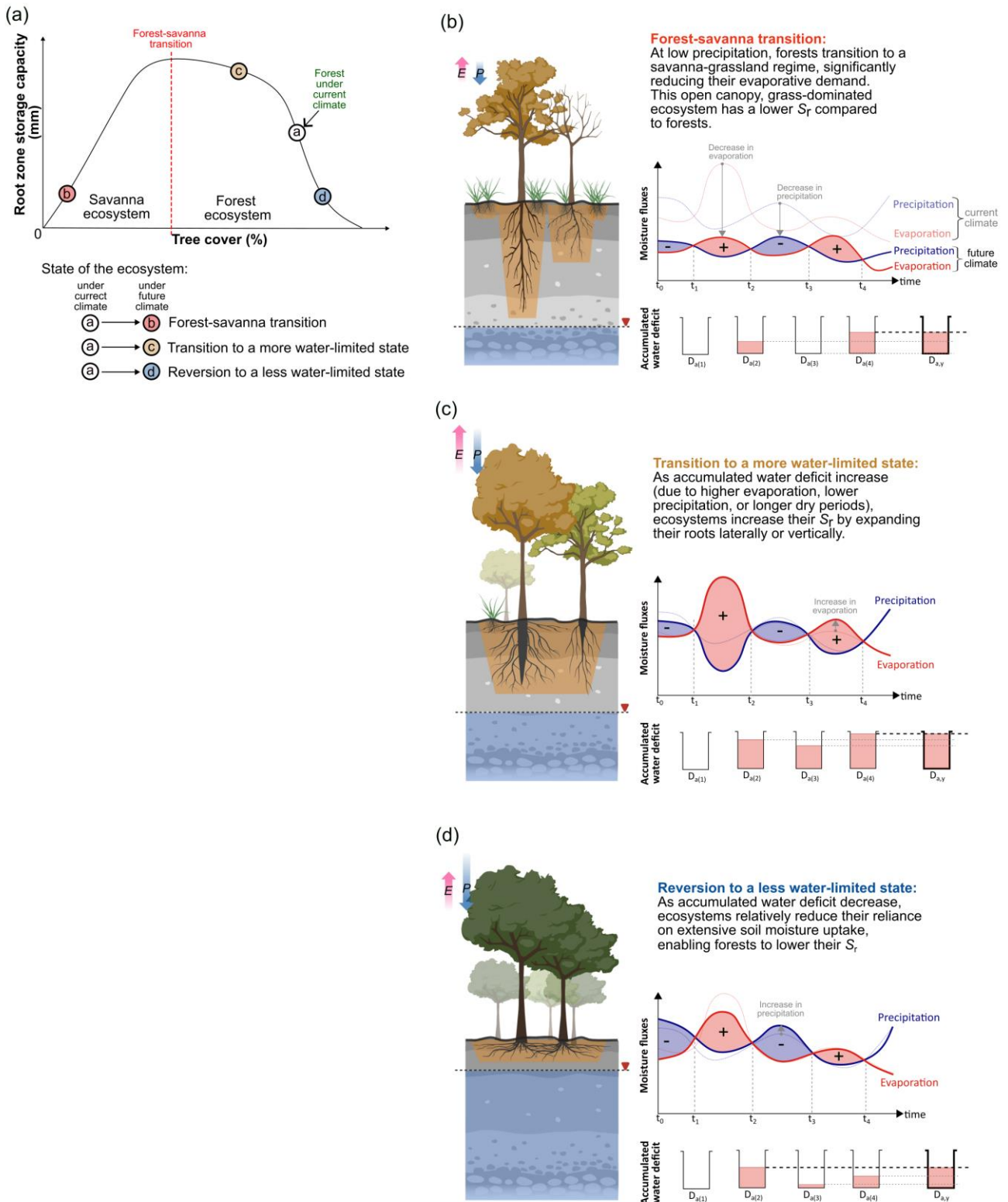
## 621 A2. Abiotic and biotic factors influence soil moisture availability

622 In this study,  $S_r$  quantifies the hydrological buffer necessary for an ecosystem to maintain its structure and  
 623 functions, reflecting the amount of root zone soil moisture available to vegetation for transpiration. Our mass-  
 624 balance-based  $S_r$  methodology, while not directly distinguishing between the biotic and abiotic influences on soil  
 625 moisture and root characteristics, does incorporate their critical role in shaping the ecohydrology of the ecosystem  
 626 under climate change. By utilising empirical precipitation and evaporation data, our approach theoretically  
 627 captures the combined impact of these biotic and abiotic factors on the actual hydrological regime (including soil  
 628 moisture) of the ecosystem (Sect. 2.3.2).

629 We acknowledge that abiotic factors such as soil texture, structure, and depth profoundly affect soil  
 630 water-holding capacity (Fayos, 1997). For instance, field studies suggest that clay and organic-rich soils exhibit  
 631 superior water retention capabilities due to their fine textures and high surface areas, **which is** crucial to vegetation  
 632 for moisture uptake during extended dry periods (Bronick and Lal, 2005; Fayos, 1997). Additionally, the depth  
 633 and porosity of soil also dictate its ability to absorb and store water in the soil, with deeper, less compacted soils  
 634 providing a higher buffer against drought by allowing greater water infiltration (Indoria et al., 2020; Smith et al.,  
 635 2001). ~~Climate change, b~~By altering temperature and precipitation patterns, **climate change** can modify these  
 636 abiotic soil properties, potentially leading to **a** loss in soil water retention capacity through erosion and  
 637 compaction (Dexter, 2004).

638 Moreover, biotic factors, including plant-root dynamics and microbial activity, also play essential roles  
 639 in shaping the ecosystem (Brunner et al., 2015; Sveen et al., 2024). Deep and extensive root systems not only  
 640 directly improve access to deeper soil moisture, but also physically modify the soil to enhance its permeability

641 and storage (Canadell et al., 1996; Jackson et al., 1996). Additionally, microbial processes contribute by breaking  
642 down organic matter, thereby improving the soil's structural integrity and ability to retain water (Dittert et al.,  
643 2006). These biotic interactions, coupled with changing abiotic factors under climate change, underscore the  
644 complex dynamics that govern soil moisture availability and ecosystem resilience. However, this study does not  
645 consider the direct impact of future climate change on biotic and abiotic factors, nor their influence on  
646 ecosystems, beyond changes to  $S_r$ .



647

648 **Figure A2:** (a) The figure compares the root zone storage capacity ( $S_r$ ) with the ecosystem state (i.e., tree cover).  
 649 This figure expands on the conceptual illustration from Fig. A1, showing how the ecosystem's precipitation and  
 650 evaporation fluxes contribute to  $S_r$  under different forest transition scenarios: (b) forest-savanna transition, (c)  
 651 transition to a more water-limited state, and (d) reversion to a less water-limited state.

652



### 653 **A3. Using precipitation to discern savanna from forests under future climate change**

654 Under future climate change, some ecosystems will remain forest, while others may transition to savanna.  
655 In our  $S_r$ -based framework, without information about above-ground forest structure, it is difficult to discern  
656 whether an ecosystem is a forest or savanna just with  $S_r$  (for instance, an ecosystem with  $S_r$  of 200 mm can either  
657 be a moderately water-limited forest or savanna; Sect. 2.3.2). Differentiating these ecosystems is easier under the  
658 current climate, where we have several remote sensing products capturing vegetation structure (e.g., tree cover  
659 density, tree height, floristic patterns) (Aleman et al., 2020; Hirota et al., 2011; Xu et al., 2016). However, under  
660 future climate, we must find a proxy, since land-use information in ESMs ~~are~~is prescribed (i.e., not biophysically  
661 simulated) (Ma et al., 2020).

662 To address this, previous studies have either relied on vegetation structure proxies provided by ESMs (e.g.,  
663 net primary productivity) (Boulton et al., 2013; Jones et al., 2009); or assumed that terrestrial ecosystems are in  
664 equilibrium with their climate (Staal et al., 2020) (see Supplement). In this study, we adopted the latter approach  
665 and utilised climate variables, specifically (bias-corrected) mean annual precipitation and the precipitation  
666 seasonality index, as proxies to make this distinction (Fig. S4). The climate conditions (or range) necessary for  
667 forest ecosystems to sustain themselves are determined by comparing empirical estimates of mean annual  
668 precipitation and precipitation seasonality index with  $S_r$ . These estimates are then bias-corrected (following the  
669 same methods described in Sect. 2.3.3) before applying them to future climate scenarios. This (revised)  
670 classification of terrestrial ecosystems is then used to assess forest transitions under future climate change  
671 scenarios.

672

## 673 **Appendix B: Results**

### 674 **B1. Sensitivity analysis reveals robust performance of the framework**

675 Sensitivity analysis reveals that by setting an extreme  $S_r$  threshold – signifying a forest-savanna transition for  
676 ecosystems that cannot maintain their above-ground structure at high  $S_r$  – we observe some shifts near the already  
677 projected risk regions and coastal areas (Fig. 3 and Fig. S18). However, the transition risk identified in the coastal  
678 regions may be an artefact of interpolating hydroclimate estimates to higher resolution. Additionally, since  
679 evaporation is more prevalent over oceans than land, this could result in high  $S_r$  values, thereby projecting an  
680 elevated tipping risk in these coastal areas.

681 We also discover that variations in the evaporation datasets and return periods used for calculating  $S_r$   
682 have minimal effect on forest transitions (Fig. S19 and S20). Although the forest classification thresholds may  
683 shift with different evaporation products under current climate conditions (Singh et al., 2020), our histogram  
684 equivalence method ensures that forest classifications under future climates adjust accordingly, resulting in only  
685 minor alterations to the final outcome (Fig. 1b and Fig. S19). Furthermore, while  $S_r$  values tend to increase with  
686 increase with shorter return periods, the impact of these changes becomes less significant with longer return  
687 periods (Wang-Erlandsson et al., 2016), leading to minor variations in the end results (Fig. S20).

688           Moreover, lowering the forest-savanna transition thresholds can reduce the risk of forest-savanna  
689 transition since it expands the associated range of climate conditions (i.e., mean annual precipitation and  
690 seasonality) necessary for forests to sustain their structure and functions (Fig. S21). Conversely, increasing the  
691 forest-savanna transition threshold leads to an opposite trend, where the risk of transition increases (Fig. S22).  
692 Despite these sensitivity analyses, the variation in transition magnitudes is minor, and the trends across different  
693 SSP scenarios for both continents remain consistent (Fig. 2 and Fig. S18-S22). Therefore, the conclusions drawn  
694 from this study remain robust, even with variations in factors that could potentially affect forest transitions.

## 695 **Data availability**

696 All the data generated during this study is made publicly available at Zenodo:  
697 <https://zenodo.org/record/7706640>. Other datasets that support the findings of this study are publicly available  
698 at: (CMIP6; citations referred to in Table S2) <https://aims2.llnl.gov/>, (Root zone storage capacity; empirical)  
699 <https://github.com/chandrakant6492/Drought-coping-strategy>, (P-CHIRPS)  
700 <https://data.chc.ucsb.edu/products/CHIRPS-2.0/>, (E-BESS) <ftp://147.46.64.183/>, (E-FLUXCOM) [ftp.bgc-](ftp.bgc-jena.mpg.de)  
701 [jena.mpg.de](ftp.bgc-jena.mpg.de), (E-PML) <https://data.csiro.au/collections/#collection/CIcsiro:17375v2>, (E-ERA5)  
702 <https://cds.climate.copernicus.eu/cdsapp#!/dataset/reanalysis-era5-single-levels>, (Globcover)  
703 [http://due.esrin.esa.int/page\\_globcover.php](http://due.esrin.esa.int/page_globcover.php). Potential transitions for each ESM based on the comparison  
704 between empirical (2001-2012) and SSP (2086-2100) scenarios are presented in the Supplement.

## 705 **Code availability**

706 The python-language scripts used for the analyses presented in this study are available from GitHub:  
707 <https://github.com/chandrakant6492/Future-forest-transitions-CMIP6>. The python-language code for  
708 calculating (empirical) root zone storage capacity is available from GitHub:  
709 <https://github.com/chandrakant6492/Drought-coping-strategy>.

## 710 **Acknowledgements**

711 C.S., I.F. and L.W.-E. acknowledge funding support from the European Research Council (ERC) project ‘Earth  
712 Resilience in the Anthropocene’, project number ERC-2016-ADG-743080. L.W.-E. also acknowledges funding  
713 support from the Swedish Research Council for Sustainable Development (FORMAS), project number 2019-  
714 01220 and the IKEA Foundation. R.v.d.E. acknowledges funding support from the Netherlands Organisation for  
715 Scientific Research (NWO), project number 016.Veni.181.015. The authors also acknowledge the computational  
716 support provided by Microsoft Planetary Computer (<https://planetarycomputer.microsoft.com>) for performing  
717 the analyses.

## 718 **Author contributions**

719 All authors contributed to the conceptualisation of this research. CS performed the analyses and wrote the initial  
720 draft. All authors contributed to the discussion and revisions, leading to the final version of the manuscript.

## 721 **Competing interests**

722 The authors declare no competing interests.

723

724

725 **References**

- 726 Ahlström, A., Canadell, J. G., Schurgers, G., Wu, M., Berry, J. A., Guan, K., and Jackson, R. B.: Hydrologic  
727 resilience and Amazon productivity, *Nature Communications*, 8, 387, [https://doi.org/10.1038/s41467-017-](https://doi.org/10.1038/s41467-017-00306-z)  
728 00306-z, 2017.
- 729 Albasha, R., Mailhol, J.-C., and Cheviron, B.: Compensatory uptake functions in empirical macroscopic root  
730 water uptake models – Experimental and numerical analysis, *Agricultural Water Management*, 155, 22–39,  
731 <https://doi.org/10.1016/j.agwat.2015.03.010>, 2015.
- 732 Aleman, J. C., Fayolle, A., Favier, C., Staver, A. C., Dexter, K. G., Ryan, C. M., Azihou, A. F., Bauman, D.,  
733 Beest, M. te, Chidumayo, E. N., Comiskey, J. A., Cromsigt, J. P. G. M., Dessard, H., Doucet, J.-L., Finckh, M.,  
734 Gillet, J.-F., Gourlet-Fleury, S., Hempson, G. P., Holdo, R. M., Kirunda, B., Kouame, F. N., Mahy, G.,  
735 Gonçalves, F. M. P., McNicol, I., Quintano, P. N., Plumptre, A. J., Pritchard, R. C., Revermann, R., Schmitt, C.  
736 B., Swemmer, A. M., Talila, H., Woollen, E., and Swaine, M. D.: Floristic evidence for alternative biome states  
737 in tropical Africa, *PNAS*, 117, 28183–28190, <https://doi.org/10.1073/pnas.2011515117>, 2020.
- 738 Anderegg, W. R. L., Klein, T., Bartlett, M., Sack, L., Pellegrini, A. F. A., Choat, B., and Jansen, S.: Meta-  
739 analysis reveals that hydraulic traits explain cross-species patterns of drought-induced tree mortality across the  
740 globe, *PNAS*, 113, 5024–5029, <https://doi.org/10.1073/pnas.1525678113>, 2016.
- 741 Armstrong McKay, D. I., Staal, A., Abrams, J. F., Winkelmann, R., Sakschewski, B., Loriani, S., Fetzer, I.,  
742 Cornell, S. E., Rockström, J., and Lenton, T. M.: Exceeding 1.5°C global warming could trigger multiple  
743 climate tipping points, *Science*, 377, eabn7950, <https://doi.org/10.1126/science.abn7950>, 2022.
- 744 Arora, V. K., Seiler, C., Wang, L., and Kou-Giesbrecht, S.: Towards an ensemble-based evaluation of land  
745 surface models in light of uncertain forcings and observations, *Biogeosciences*, 20, 1313–1355,  
746 <https://doi.org/10.5194/bg-20-1313-2023>, 2023.
- 747 Baker, J. C. A., Garcia-Carreras, L., Buermann, W., Souza, D. C. de, Marsham, J. H., Kubota, P. Y., Gloor, M.,  
748 Coelho, C. A. S., and Spracklen, D. V.: Robust Amazon precipitation projections in climate models that capture  
749 realistic land–atmosphere interactions, *Environ. Res. Lett.*, 16, 074002, [https://doi.org/10.1088/1748-](https://doi.org/10.1088/1748-9326/abfb2e)  
750 9326/abfb2e, 2021.
- 751 Barros, F. de V., Bittencourt, P. R. L., Brum, M., Restrepo-Coupe, N., Pereira, L., Teodoro, G. S., Saleska, S.  
752 R., Borma, L. S., Christoffersen, B. O., Penha, D., Alves, L. F., Lima, A. J. N., Carneiro, V. M. C., Gentine, P.,  
753 Lee, J.-E., Aragão, L. E. O. C., Ivanov, V., Leal, L. S. M., Araujo, A. C., and Oliveira, R. S.: Hydraulic traits  
754 explain differential responses of Amazonian forests to the 2015 El Niño-induced drought, *New Phytologist*,  
755 223, 1253–1266, <https://doi.org/10.1111/nph.15909>, 2019.
- 756 Bauman, D., Fortunel, C., Delhaye, G., Malhi, Y., Cernusak, L. A., Bentley, L. P., Rifai, S. W., Aguirre-  
757 Gutiérrez, J., Menor, I. O., Phillips, O. L., McNellis, B. E., Bradford, M., Laurance, S. G. W., Hutchinson, M.  
758 F., Dempsey, R., Santos-Andrade, P. E., Ninantay-Rivera, H. R., Chambi Paucar, J. R., and McMahon, S. M.:  
759 Tropical tree mortality has increased with rising atmospheric water stress, *Nature*, 1–6,  
760 <https://doi.org/10.1038/s41586-022-04737-7>, 2022.
- 761 de Boer-Euser, T., McMillan, H. K., Hrachowitz, M., Winsemius, H. C., and Savenije, H. H. G.: Influence of  
762 soil and climate on root zone storage capacity, *Water Resources Research*, 52, 2009–2024,  
763 <https://doi.org/10.1002/2015WR018115>, 2016.
- 764 Bouaziz, L. J. E., Steele-Dunne, S. C., Schellekens, J., Weerts, A. H., Stam, J., Sprokkereef, E., Winsemius, H.  
765 H. C., Savenije, H. H. G., and Hrachowitz, M.: Improved Understanding of the Link Between Catchment-Scale  
766 Vegetation Accessible Storage and Satellite-Derived Soil Water Index, *Water Resources Research*, 56,  
767 e2019WR026365, <https://doi.org/10.1029/2019WR026365>, 2020.

- 768 Boulton, C. A., Good, P., and Lenton, T. M.: Early warning signals of simulated Amazon rainforest dieback,  
769 *Theor Ecol*, 6, 373–384, <https://doi.org/10.1007/s12080-013-0191-7>, 2013.
- 770 Boulton, C. A., Booth, B. B. B., and Good, P.: Exploring uncertainty of Amazon dieback in a perturbed  
771 parameter Earth system ensemble, *Global Change Biology*, 23, 5032–5044, <https://doi.org/10.1111/gcb.13733>,  
772 2017.
- 773 Boulton, C. A., Lenton, T. M., and Boers, N.: Pronounced loss of Amazon rainforest resilience since the early  
774 2000s, *Nat. Clim. Chang.*, 12, 271–278, <https://doi.org/10.1038/s41558-022-01287-8>, 2022.
- 775 Bovolo, C. I., Wagner, T., Parkin, G., Hein-Griggs, D., Pereira, R., and Jones, R.: The Guiana Shield  
776 rainforests—overlooked guardians of South American climate, *Environ. Res. Lett.*, 13, 074029,  
777 <https://doi.org/10.1088/1748-9326/aacf60>, 2018.
- 778 Brienen, R. J. W., Phillips, O. L., Feldpausch, T. R., Gloor, E., Baker, T. R., Lloyd, J., Lopez-Gonzalez, G.,  
779 Monteagudo-Mendoza, A., Malhi, Y., Lewis, S. L., Vásquez Martínez, R., Alexiades, M., Álvarez Dávila, E.,  
780 Alvarez-Loayza, P., Andrade, A., Aragão, L. E. O. C., Araujo-Murakami, A., Arets, E. J. M. M., Arroyo, L.,  
781 Aymard C., G. A., Bánki, O. S., Baraloto, C., Barroso, J., Bonal, D., Boot, R. G. A., Camargo, J. L. C.,  
782 Castilho, C. V., Chama, V., Chao, K. J., Chave, J., Comiskey, J. A., Cornejo Valverde, F., da Costa, L., de  
783 Oliveira, E. A., Di Fiore, A., Erwin, T. L., Fauset, S., Forsthofer, M., Galbraith, D. R., Grahame, E. S., Groot,  
784 N., Hérault, B., Higuchi, N., Honorio Coronado, E. N., Keeling, H., Killeen, T. J., Laurance, W. F., Laurance,  
785 S., Licona, J., Magnussen, W. E., Marimon, B. S., Marimon-Junior, B. H., Mendoza, C., Neill, D. A., Nogueira,  
786 E. M., Núñez, P., Pallqui Camacho, N. C., Parada, A., Pardo-Molina, G., Peacock, J., Peña-Claros, M.,  
787 Pickavance, G. C., Pitman, N. C. A., Poorter, L., Prieto, A., Quesada, C. A., Ramírez, F., Ramírez-Angulo, H.,  
788 Restrepo, Z., Roopsind, A., Rudas, A., Salomão, R. P., Schwarz, M., Silva, N., Silva-Espejo, J. E., Silveira, M.,  
789 Stropp, J., Talbot, J., ter Steege, H., Teran-Aguilar, J., Terborgh, J., Thomas-Caesar, R., Toledo, M., Torello-  
790 Raventos, M., Umetsu, R. K., van der Heijden, G. M. F., van der Hout, P., Guimarães Vieira, I. C., Vieira, S.  
791 A., Vilanova, E., Vos, V. A., and Zagt, R. J.: Long-term decline of the Amazon carbon sink, *Nature*, 519, 344–  
792 348, <https://doi.org/10.1038/nature14283>, 2015.
- 793 Bronick, C. J. and Lal, R.: Soil structure and management: a review, *Geoderma*, 124, 3–22,  
794 <https://doi.org/10.1016/j.geoderma.2004.03.005>, 2005.
- 795 Brooks, P. D., Chorover, J., Fan, Y., Godsey, S. E., Maxwell, R. M., McNamara, J. P., and Tague, C.:  
796 Hydrological partitioning in the critical zone: Recent advances and opportunities for developing transferable  
797 understanding of water cycle dynamics, *Water Resources Research*, 51, 6973–6987,  
798 <https://doi.org/10.1002/2015WR017039>, 2015.
- 799 Brum, M., Vadeboncoeur, M. A., Ivanov, V., Asbjornsen, H., Saleska, S., Alves, L. F., Penha, D., Dias, J. D.,  
800 Aragão, L. E. O. C., Barros, F., Bittencourt, P., Pereira, L., and Oliveira, R. S.: Hydrological niche segregation  
801 defines forest structure and drought tolerance strategies in a seasonal Amazon forest, *Journal of Ecology*, 107,  
802 318–333, <https://doi.org/10.1111/1365-2745.13022>, 2019.
- 803 Brunner, I., Herzog, C., Dawes, M. A., Arend, M., and Sperisen, C.: How tree roots respond to drought,  
804 *Frontiers in Plant Science*, 6, 2015.
- 805 Bruno, R. D., Rocha, H. R. da, Freitas, H. C. de, Goulden, M. L., and Miller, S. D.: Soil moisture dynamics in  
806 an eastern Amazonian tropical forest, *Hydrological Processes*, 20, 2477–2489,  
807 <https://doi.org/10.1002/hyp.6211>, 2006.
- 808 Canadell, J., Jackson, R. B., Ehleringer, J. B., Mooney, H. A., Sala, O. E., and Schulze, E.-D.: Maximum  
809 rooting depth of vegetation types at the global scale, *Oecologia*, 108, 583–595,  
810 <https://doi.org/10.1007/BF00329030>, 1996.

811 Canadell, J. G., Monteiro, P. M. S., Costa, M. H., Cunha, L. C. D., Cox, P. M., Eliseev, A. V., Henson, S., Ishii,  
812 M., Jaccard, S., Koven, C., Lohila, A., Patra, P. K., Piao, S., Syampungani, S., Zaehle, S., Zickfeld, K.,  
813 Alexandrov, G. A., Bala, G., Bopp, L., Boysen, L., Cao, L., Chandra, N., Ciais, P., Denisov, S. N., Dentener, F.  
814 J., Douville, H., Fay, A., Forster, P., Fox-Kemper, B., Friedlingstein, P., Fu, W., Fuss, S., Garçon, V., Gier, B.,  
815 Gillett, N. P., Gregor, L., Haustein, K., Haverd, V., He, J., Hewitt, H. T., Hoffman, F. M., Ilyina, T., Jackson,  
816 R., Jones, C., Keller, D. P., Kwiatkowski, L., Lamboll, R. D., Lan, X., Laufkötter, C., Quéré, C. L., Lenton, A.,  
817 Lewis, J., Liddicoat, S., Lorenzoni, L., Lovenduski, N., Macdougall, A. H., Mathesius, S., Matthews, D. H.,  
818 Meinshausen, M., Mokhov, I. I., Naik, V., Nicholls, Z. R. J., Nurhati, I. S., O'sullivan, M., Peters, G., Pongratz,  
819 J., Poulter, B., Sallée, J.-B., Saunio, M., Schuur, E. A. G., I.Seneviratne, S., Stavert, A., Suntharalingam, P.,  
820 Tachiiri, K., Terhaar, J., Thompson, R., Tian, H., Turnbull, J., Vicente-Serrano, S. M., Wang, X., Wanninkhof,  
821 R. H., Williamson, P., Brovkin, V., Feely, R. A., and Lebehof, A. D.: Global Carbon and other Biogeochemical  
822 Cycles and Feedbacks, in: IPCC AR6 WGI, Final Government Distribution, chapter 5, 2021.

823 Chai, Y., Martins, G., Nobre, C., von Randow, C., Chen, T., and Dolman, H.: Constraining Amazonian land  
824 surface temperature sensitivity to precipitation and the probability of forest dieback, *npj Clim Atmos Sci*, 4, 1–  
825 7, <https://doi.org/10.1038/s41612-021-00162-1>, 2021.

826 Cheng, S., Huang, J., Ji, F., and Lin, L.: Uncertainties of soil moisture in historical simulations and future  
827 projections, *Journal of Geophysical Research: Atmospheres*, 122, 2239–2253,  
828 <https://doi.org/10.1002/2016JD025871>, 2017.

829 Cole, L. E. S., Bhagwat, S. A., and Willis, K. J.: Recovery and resilience of tropical forests after disturbance,  
830 *Nature Communications*, 5, 3906, <https://doi.org/10.1038/ncomms4906>, 2014.

831 Condit, R., Engelbrecht, B. M. J., Pino, D., Pérez, R., and Turner, B. L.: Species distributions in response to  
832 individual soil nutrients and seasonal drought across a community of tropical trees, *PNAS*, 110, 5064–5068,  
833 <https://doi.org/10.1073/pnas.1218042110>, 2013.

834 Cook, K. H. and Vizy, E. K.: Impact of climate change on mid-twenty-first century growing seasons in Africa,  
835 *Clim Dyn*, 39, 2937–2955, <https://doi.org/10.1007/s00382-012-1324-1>, 2012.

836 Cooper, G. S., Willcock, S., and Dearing, J. A.: Regime shifts occur disproportionately faster in larger  
837 ecosystems, *Nature Communications*, 11, 1175, <https://doi.org/10.1038/s41467-020-15029-x>, 2020.

838 skextremes Documentation: <https://github.com/kikocorreoso/scikit-extremes>.

839 Cox, P. M., Betts, R. A., Collins, M., Harris, P. P., Huntingford, C., and Jones, C. D.: Amazonian forest  
840 dieback under climate-carbon cycle projections for the 21st century, *Theor Appl Climatol*, 78, 137–156,  
841 <https://doi.org/10.1007/s00704-004-0049-4>, 2004.

842 Dai, A.: Drought under global warming: a review, *WIREs Climate Change*, 2, 45–65,  
843 <https://doi.org/10.1002/wcc.81>, 2011.

844 Davidson, E. A., de Araújo, A. C., Artaxo, P., Balch, J. K., Brown, I. F., C. Bustamante, M. M., Coe, M. T.,  
845 DeFries, R. S., Keller, M., Longo, M., Munger, J. W., Schroeder, W., Soares-Filho, B. S., Souza, C. M., and  
846 Wofsy, S. C.: The Amazon basin in transition, *Nature*, 481, 321–328, <https://doi.org/10.1038/nature10717>,  
847 2012.

848 Dexter, A. R.: Soil physical quality: Part II. Friability, tillage, tilth and hard-setting, *Geoderma*, 120, 215–225,  
849 <https://doi.org/10.1016/j.geoderma.2003.09.005>, 2004.

850 Dittert, K., Wätzel, J., and Sattelmacher, B.: Responses of *Alnus glutinosa* to Anaerobic Conditions -  
851 Mechanisms and Rate of Oxygen Flux into the Roots, *Plant Biology*, 8, 212–223, [https://doi.org/10.1055/s-](https://doi.org/10.1055/s-2005-873041)  
852 2005-873041, 2006.

- 853 Doughty, C. E., Keany, J. M., Wiebe, B. C., Rey-Sanchez, C., Carter, K. R., Middleby, K. B., Cheesman, A.  
854 W., Goulden, M. L., da Rocha, H. R., Miller, S. D., Malhi, Y., Fauset, S., Gloor, E., Slot, M., Oliveras Menor,  
855 I., Crous, K. Y., Goldsmith, G. R., and Fisher, J. B.: Tropical forests are approaching critical temperature  
856 thresholds, *Nature*, 621, 105–111, <https://doi.org/10.1038/s41586-023-06391-z>, 2023.
- 857 Driyfhout, S., Bathiany, S., Beaulieu, C., Brovkin, V., Claussen, M., Huntingford, C., Scheffer, M., Sgubin, G.,  
858 and Swingedouw, D.: Catalogue of abrupt shifts in Intergovernmental Panel on Climate Change climate  
859 models, *Proceedings of the National Academy of Sciences*, 112, E5777–E5786,  
860 <https://doi.org/10.1073/pnas.1511451112>, 2015.
- 861 Dunning, C. M., Black, E., and Allan, R. P.: Later Wet Seasons with More Intense Rainfall over Africa under  
862 Future Climate Change, *Journal of Climate*, 31, 9719–9738, 2018.
- 863 van der Ent, R. J., Savenije, H. H. G., Schaeffli, B., and Steele-Dunne, S. C.: Origin and fate of atmospheric  
864 moisture over continents, *Water Resources Research*, 46, <https://doi.org/10.1029/2010WR009127>, 2010.
- 865 GlobCover land-use map: [http://due.esrin.esa.int/page\\_globcover.php](http://due.esrin.esa.int/page_globcover.php), last access: 27 February 2022.
- 866 Esquivel-Muelbert, A., Baker, T. R., Dexter, K. G., Lewis, S. L., Brienen, R. J. W., Feldpausch, T. R., Lloyd,  
867 J., Monteagudo-Mendoza, A., Arroyo, L., Álvarez-Dávila, E., Higuchi, N., Marimon, B. S., Marimon-Junior,  
868 B. H., Silveira, M., Vilanova, E., Gloor, E., Malhi, Y., Chave, J., Barlow, J., Bonal, D., Cardozo, N. D., Erwin,  
869 T., Fauset, S., Hérault, B., Laurance, S., Poorter, L., Qie, L., Stahl, C., Sullivan, M. J. P., Steege, H. ter, Vos, V.  
870 A., Zuidema, P. A., Almeida, E., Oliveira, E. A. de, Andrade, A., Vieira, S. A., Aragão, L., Araujo-Murakami,  
871 A., Arets, E., C. G. A. A., Baraloto, C., Camargo, P. B., Barroso, J. G., Bongers, F., Boot, R., Camargo, J. L.,  
872 Castro, W., Moscoso, V. C., Comiskey, J., Valverde, F. C., Costa, A. C. L. da, Pasquel, J. del A., Fiore, A. D.,  
873 Duque, L. F., Elias, F., Engel, J., Llampazo, G. F., Galbraith, D., Fernández, R. H., Coronado, E. H., Hubau,  
874 W., Jimenez-Rojas, E., Lima, A. J. N., Umetsu, R. K., Laurance, W., Lopez-Gonzalez, G., Lovejoy, T., Cruz,  
875 O. A. M., Morandi, P. S., Neill, D., Vargas, P. N., Camacho, N. C. P., Gutierrez, A. P., Pardo, G., Peacock, J.,  
876 Peña-Claros, M., Peñuela-Mora, M. C., Petronelli, P., Pickavance, G. C., Pitman, N., Prieto, A., Quesada, C.,  
877 Ramírez-Angulo, H., Réjou-Méchain, M., Correa, Z. R., Roopsind, A., Rudas, A., Salomão, R., Silva, N.,  
878 Espejo, J. S., Singh, J., Stropp, J., Terborgh, J., Thomas, R., Toledo, M., Torres-Lezama, A., Gamarra, L. V.,  
879 Meer, P. J. van de, Heijden, G. van der, et al.: Compositional response of Amazon forests to climate change,  
880 *Global Change Biology*, 25, 39–56, <https://doi.org/10.1111/gcb.14413>, 2019.
- 881 Fan, Y., Miguez-Macho, G., Jobbágy, E. G., Jackson, R. B., and Otero-Casal, C.: Hydrologic regulation of  
882 plant rooting depth, *Proceedings of the National Academy of Sciences*, 114, 10572–10577,  
883 <https://doi.org/10.1073/pnas.1712381114>, 2017.
- 884 Fayos, C. B.: The roles of texture and structure in the water retention capacity of burnt Mediterranean soils with  
885 varying rainfall, *CATENA*, 31, 219–236, [https://doi.org/10.1016/S0341-8162\(97\)00041-6](https://doi.org/10.1016/S0341-8162(97)00041-6), 1997.
- 886 February, E. C. and Higgins, S. I.: The distribution of tree and grass roots in savannas in relation to soil  
887 nitrogen and water, *South African Journal of Botany*, 76, 517–523, <https://doi.org/10.1016/j.sajb.2010.04.001>,  
888 2010.
- 889 Ferreira, D., Marshall, J., and Rose, B.: Climate Determinism Revisited: Multiple Equilibria in a Complex  
890 Climate Model, *Journal of Climate*, 24, 992–1012, <https://doi.org/10.1175/2010JCLI3580.1>, 2011.
- 891 Fleischer, K., Rammig, A., De Kauwe, M. G., Walker, A. P., Domingues, T. F., Fuchslueger, L., Garcia, S.,  
892 Goll, D. S., Grandis, A., Jiang, M., Haverd, V., Hofhansl, F., Holm, J. A., Kruijt, B., Leung, F., Medlyn, B. E.,  
893 Mercado, L. M., Norby, R. J., Pak, B., von Randow, C., Quesada, C. A., Schaap, K. J., Valverde-Barrantes, O.  
894 J., Wang, Y.-P., Yang, X., Zaehle, S., Zhu, Q., and Lapola, D. M.: Amazon forest response to CO<sub>2</sub> fertilization  
895 dependent on plant phosphorus acquisition, *Nat. Geosci.*, 12, 736–741, <https://doi.org/10.1038/s41561-019-0404-9>,  
896 2019.

- 897 Flores, B. M., Montoya, E., Sakschewski, B., Nascimento, N., Staal, A., Betts, R. A., Levis, C., Lapola, D. M.,  
898 Esquivel-Muelbert, A., Jakovac, C., Nobre, C. A., Oliveira, R. S., Borma, L. S., Nian, D., Boers, N., Hecht, S.  
899 B., ter Steege, H., Arriera, J., Lucas, I. L., Berenguer, E., Marengo, J. A., Gatti, L. V., Mattos, C. R. C., and  
900 Hirota, M.: Critical transitions in the Amazon forest system, *Nature*, 626, 555–564,  
901 <https://doi.org/10.1038/s41586-023-06970-0>, 2024.
- 902 Funk, C., Peterson, P., Landsfeld, M., Pedreros, D., Verdin, J., Shukla, S., Husak, G., Rowland, J., Harrison, L.,  
903 Hoell, A., and Michaelsen, J.: The climate hazards infrared precipitation with stations—a new environmental  
904 record for monitoring extremes, *Scientific Data*, 2, 150066, <https://doi.org/10.1038/sdata.2015.66>, 2015.
- 905 Gao, H., Hrachowitz, M., Schymanski, S. J., Fenicia, F., Sriwongsitanon, N., and Savenije, H. H. G.: Climate  
906 controls how ecosystems size the root zone storage capacity at catchment scale: Root zone storage capacity in  
907 catchments, *Geophysical Research Letters*, 41, 7916–7923, <https://doi.org/10.1002/2014GL061668>, 2014.
- 908 Grimm, N. B., Chapin III, F. S., Bierwagen, B., Gonzalez, P., Groffman, P. M., Luo, Y., Melton, F.,  
909 Nadelhoffer, K., Pairis, A., Raymond, P. A., Schimel, J., and Williamson, C. E.: The impacts of climate change  
910 on ecosystem structure and function, *Frontiers in Ecology and the Environment*, 11, 474–482,  
911 <https://doi.org/10.1890/120282>, 2013.
- 912 Gumbel, E. J.: *Statistics of extremes.*, Columbia University Press, New York, 1958.
- 913 Guswa, A. J.: The influence of climate on root depth: A carbon cost-benefit analysis, *Water Resources*  
914 *Research*, 44, W02427, <https://doi.org/10.1029/2007WR006384>, 2008.
- 915 Hahm, W. J., Rempe, D. M., Dralle, D. N., Dawson, T. E., Lovill, S. M., Bryk, A. B., Bish, D. L., Schieber, J.,  
916 and Dietrich, W. E.: Lithologically Controlled Subsurface Critical Zone Thickness and Water Storage Capacity  
917 Determine Regional Plant Community Composition, *Water Resources Research*, 55, 3028–3055,  
918 <https://doi.org/10.1029/2018WR023760>, 2019.
- 919 Hall, A., Cox, P., Huntingford, C., and Klein, S.: Progressing emergent constraints on future climate change,  
920 *Nat. Clim. Chang.*, 9, 269–278, <https://doi.org/10.1038/s41558-019-0436-6>, 2019.
- 921 Hersbach, H., Bell, B., Berrisford, P., Hirahara, S., Horányi, A., Muñoz-Sabater, J., Nicolas, J., Peubey, C.,  
922 Radu, R., Schepers, D., Simmons, A., Soci, C., Abdalla, S., Abellan, X., Balsamo, G., Bechtold, P., Biavati, G.,  
923 Bidlot, J., Bonavita, M., Chiara, G. D., Dahlgren, P., Dee, D., Diamantakis, M., Dragani, R., Flemming, J.,  
924 Forbes, R., Fuentes, M., Geer, A., Haimberger, L., Healy, S., Hogan, R. J., Hólm, E., Janisková, M., Keeley, S.,  
925 Laloyaux, P., Lopez, P., Lupu, C., Radnoti, G., Rosnay, P. de, Rozum, I., Vamborg, F., Villaume, S., and  
926 Thépaut, J.-N.: The ERA5 Global Reanalysis, *Quarterly Journal of the Royal Meteorological Society*, 245,  
927 111840, <https://doi.org/10.1002/qj.3803>, 2020.
- 928 Higgins, S. I. and Scheiter, S.: Atmospheric CO<sub>2</sub> forces abrupt vegetation shifts locally, but not globally,  
929 *Nature*, 488, 209–212, <https://doi.org/10.1038/nature11238>, 2012.
- 930 Hildebrandt, A., Kleidon, A., and Bechmann, M.: A thermodynamic formulation of root water uptake,  
931 *Hydrology and Earth System Sciences*, 20, 3441–3454, <https://doi.org/10.5194/hess-20-3441-2016>, 2016.
- 932 Hirota, M., Holmgren, M., Van Nes, E. H., and Scheffer, M.: Global Resilience of Tropical Forest and Savanna  
933 to Critical Transitions, *Science*, 334, 232–235, <https://doi.org/10.1126/science.1210657>, 2011.
- 934 Hirota, M., Flores, B. M., Betts, R., Borma, L. S., Esquivel-Muelbert, A., Jakovac, C., Lapola, D. M., Montoya,  
935 E., Oliveira, R. S., and Sakschewski, B.: Chapter 24: Resilience of the Amazon forest to global changes:  
936 Assessing the risk of tipping points, in: *Amazon Assessment Report 2021*, edited by: Nobre, C., Encalada, A.,  
937 Anderson, E., Roca Alcazar, F. H., Bustamante, M., Mena, C., Peña-Claros, M., Poveda, G., Rodriguez, J. P.,  
938 Saleska, S., Trumbore, S. E., Val, A., Villa Nova, L., Abramovay, R., Alencar, A., Rodriguez Alzza, A. C.,  
939 Armenteras, D., Artaxo, P., Athayde, S., Barretto Filho, H. T., Barlow, J., Berenguer, E., Bortolotto, F., Costa,



- 940 F. de A., Costa, M. H., Cuvi, N., Fearnside, P., Ferreira, J., Flores, B. M., Frieri, S., Gatti, L. V., Guayasamin,  
 941 J. M., Hecht, S., Hirota, M., Hoorn, C., Josse, C., Lapola, D. M., Larrea, C., Larrea-Alcazar, D. M., Lehm  
 942 Ardaya, Z., Malhi, Y., Marengo, J. A., Melack, J., Moraes R., M., Moutinho, P., Murmis, M. R., Neves, E. G.,  
 943 Paez, B., Painter, L., Ramos, A., Rosero-Peña, M. C., Schmink, M., Sist, P., ter Steege, H., Val, P., van der  
 944 Voort, H., Varese, M., and Zapata-Ríos, G., UN Sustainable Development Solutions Network (SDSN),  
 945 <https://doi.org/10.55161/QPYS9758>, 2021.
- 946 Hofhansl, F., Andersen, K. M., Fleischer, K., Fuchslueger, L., Rammig, A., Schaap, K. J., Valverde-Barrantes,  
 947 O. J., and Lapola, D. M.: Amazon Forest Ecosystem Responses to Elevated Atmospheric CO<sub>2</sub> and Alterations  
 948 in Nutrient Availability: Filling the Gaps with Model-Experiment Integration, *Frontiers in Earth Science*, 4,  
 949 2016.
- 950 Hubau, W., Lewis, S. L., Phillips, O. L., Affum-Baffoe, K., Beeckman, H., Cuní-Sánchez, A., Daniels, A. K.,  
 951 Ewango, C. E. N., Fauset, S., Mukinzi, J. M., Sheil, D., Sonké, B., Sullivan, M. J. P., Sunderland, T. C. H.,  
 952 Taedoumg, H., Thomas, S. C., White, L. J. T., Abernethy, K. A., Adu-Bredu, S., Amani, C. A., Baker, T. R.,  
 953 Banin, L. F., Baya, F., Begne, S. K., Bennett, A. C., Benedet, F., Bitariho, R., Bocko, Y. E., Boeckx, P.,  
 954 Boundja, P., Brienen, R. J. W., Brncic, T., Chezeaux, E., Chuyong, G. B., Clark, C. J., Collins, M., Comiskey,  
 955 J. A., Coomes, D. A., Dargie, G. C., de Haulleville, T., Kamdem, M. N. D., Doucet, J.-L., Esquivel-Muelbert,  
 956 A., Feldpausch, T. R., Fofanah, A., Foli, E. G., Gilpin, M., Gloor, E., Gonmadje, C., Gourlet-Fleury, S., Hall, J.  
 957 S., Hamilton, A. C., Harris, D. J., Hart, T. B., Hockemba, M. B. N., Hladik, A., Ifo, S. A., Jeffery, K. J., Jucker,  
 958 T., Yakusu, E. K., Kearsley, E., Kenfack, D., Koch, A., Leal, M. E., Levesley, A., Lindsell, J. A., Lisingo, J.,  
 959 Lopez-Gonzalez, G., Lovett, J. C., Makana, J.-R., Malhi, Y., Marshall, A. R., Martin, J., Martin, E. H., Mbayu,  
 960 F. M., Medjibe, V. P., Mihindou, V., Mitchard, E. T. A., Moore, S., Munishi, P. K. T., Bengone, N. N., Ojo, L.,  
 961 Ondo, F. E., Peh, K. S.-H., Pickavance, G. C., Poulsen, A. D., Poulsen, J. R., Qie, L., Reitsma, J., Rovero, F.,  
 962 Swaine, M. D., Talbot, J., Taplin, J., Taylor, D. M., Thomas, D. W., Toirambe, B., Mukendi, J. T., Tuagben,  
 963 D., Umunay, P. M., et al.: Asynchronous carbon sink saturation in African and Amazonian tropical forests,  
 964 *Nature*, 579, 80–87, <https://doi.org/10.1038/s41586-020-2035-0>, 2020.
- 965 Huntingford, C., Zelazowski, P., Galbraith, D., Mercado, L. M., Sitch, S., Fisher, R., Lomas, M., Walker, A. P.,  
 966 Jones, C. D., Booth, B. B. B., Malhi, Y., Hemming, D., Kay, G., Good, P., Lewis, S. L., Phillips, O. L., Atkin,  
 967 O. K., Lloyd, J., Gloor, E., Zaragoza-Castells, J., Meir, P., Betts, R., Harris, P. P., Nobre, C., Marengo, J., and  
 968 Cox, P. M.: Simulated resilience of tropical rainforests to CO<sub>2</sub>-induced climate change, *Nature Geosci*, 6, 268–  
 969 273, <https://doi.org/10.1038/ngeo1741>, 2013.
- 970 Hurtt, G. C., Chini, L., Sahajpal, R., Frohling, S., Boudris, B. L., Calvin, K., Doelman, J. C., Fisk, J.,  
 971 Fujimori, S., Klein Goldewijk, K., Hasegawa, T., Havlik, P., Heinemann, A., Humpenöder, F., Jungclaus, J.,  
 972 Kaplan, J. O., Kennedy, J., Krisztin, T., Lawrence, D., Lawrence, P., Ma, L., Mertz, O., Pongratz, J., Popp, A.,  
 973 Poulter, B., Riahi, K., Shevliakova, E., Stehfest, E., Thornton, P., Tubiello, F. N., van Vuuren, D. P., and  
 974 Zhang, X.: Harmonization of global land use change and management for the period 850–2100 (LUH2) for  
 975 CMIP6, *Geoscientific Model Development*, 13, 5425–5464, <https://doi.org/10.5194/gmd-13-5425-2020>, 2020.
- 976 Indoria, A. K., Sharma, K. L., and Reddy, K. S.: Chapter 18 - Hydraulic properties of soil under warming  
 977 climate, in: *Climate Change and Soil Interactions*, edited by: Prasad, M. N. V. and Pietrzykowski, M., Elsevier,  
 978 473–508, <https://doi.org/10.1016/B978-0-12-818032-7.00018-7>, 2020.
- 979 Jach, L., Warrach-Sagi, K., Ingwersen, J., Kaas, E., and Wulfmeyer, V.: Land Cover Impacts on Land-  
 980 Atmosphere Coupling Strength in Climate Simulations With WRF Over Europe, *Journal of Geophysical*  
 981 *Research: Atmospheres*, 125, e2019JD031989, <https://doi.org/10.1029/2019JD031989>, 2020.
- 982 Jackson, R. B., Canadell, J., Ehleringer, J. R., Mooney, H. A., Sala, O. E., and Schulze, E. D.: A global analysis  
 983 of root distributions for terrestrial biomes, *Oecologia*, 108, 389–411, <https://doi.org/10.1007/BF00333714>,  
 984 1996.

- 985 Jehn, F. U., Kemp, L., Ilin, E., Funk, C., Wang, J. R., and Breuer, L.: Focus of the IPCC Assessment Reports  
 986 Has Shifted to Lower Temperatures, *Earth's Future*, 10, e2022EF002876,  
 987 <https://doi.org/10.1029/2022EF002876>, 2022.
- 988 Jiang, C. and Ryu, Y.: Multi-scale evaluation of global gross primary productivity and evapotranspiration  
 989 products derived from Breathing Earth System Simulator (BESS), *Remote Sensing of Environment*, 186, 528–  
 990 547, <https://doi.org/10.1016/j.rse.2016.08.030>, 2016.
- 991 Jones, C., Lowe, J., Liddicoat, S., and Betts, R.: Committed terrestrial ecosystem changes due to climate  
 992 change, *Nature Geosci*, 2, 484–487, <https://doi.org/10.1038/ngeo555>, 2009.
- 993 Jung, M., Koirala, S., Weber, U., Ichii, K., Gans, F., Camps-Valls, G., Papale, D., Schwalm, C., Tramontana,  
 994 G., and Reichstein, M.: The FLUXCOM ensemble of global land-atmosphere energy fluxes, *Sci Data*, 6, 74,  
 995 <https://doi.org/10.1038/s41597-019-0076-8>, 2019.
- 996 Koch, A., Hubau, W., and Lewis, S. L.: Earth System Models Are Not Capturing Present-Day Tropical Forest  
 997 Carbon Dynamics, *Earth's Future*, 9, e2020EF001874, <https://doi.org/10.1029/2020EF001874>, 2021.
- 998 Kooperman, G. J., Chen, Y., Hoffman, F. M., Koven, C. D., Lindsay, K., Pritchard, M. S., Swann, A. L. S., and  
 999 Randerson, J. T.: Forest response to rising CO<sub>2</sub> drives zonally asymmetric rainfall change over tropical land,  
 1000 *Nature Clim Change*, 8, 434–440, <https://doi.org/10.1038/s41558-018-0144-7>, 2018.
- 1001 Körner, C.: A matter of tree longevity, *Science*, 355, 130–131, <https://doi.org/10.1126/science.aal2449>, 2017.
- 1002 Küçük, Ç., Koirala, S., Carvalhais, N., Miralles, D. G., Reichstein, M., and Jung, M.: Characterizing the  
 1003 Response of Vegetation Cover to Water Limitation in Africa Using Geostationary Satellites, *Journal of*  
 1004 *Advances in Modeling Earth Systems*, 14, e2021MS002730, <https://doi.org/10.1029/2021MS002730>, 2022.
- 1005 Kukal, M. S. and Irmak, S.: Can limits of plant available water be inferred from soil moisture distributions?,  
 1006 *Agricultural & Environmental Letters*, 8, e20113, <https://doi.org/10.1002/ael2.20113>, 2023.
- 1007 Lammertsma, E. I., Boer, H. J. de, Dekker, S. C., Dilcher, D. L., Lotter, A. F., and Wagner-Cremer, F.: Global  
 1008 CO<sub>2</sub> rise leads to reduced maximum stomatal conductance in Florida vegetation, *PNAS*, 108, 4035–4040,  
 1009 <https://doi.org/10.1073/pnas.1100371108>, 2011.
- 1010 Leite-Filho, A. T., Soares-Filho, B. S., Davis, J. L., Abrahão, G. M., and Börner, J.: Deforestation reduces  
 1011 rainfall and agricultural revenues in the Brazilian Amazon, *Nat Commun*, 12, 2591,  
 1012 <https://doi.org/10.1038/s41467-021-22840-7>, 2021.
- 1013 Lenton, T. M.: Early warning of climate tipping points, *Nature Clim Change*, 1, 201–209,  
 1014 <https://doi.org/10.1038/nclimate1143>, 2011.
- 1015 Lenton, T. M., Rockström, J., Gaffney, O., Rahmstorf, S., Richardson, K., Steffen, W., and Schellnhuber, H. J.:  
 1016 Climate tipping points — too risky to bet against, *Nature*, 575, 592–595, <https://doi.org/10.1038/d41586-019-03595-0>, 2019.
- 1018 Lewis, S. L., Edwards, D. P., and Galbraith, D.: Increasing human dominance of tropical forests, *Science*, 349,  
 1019 827–832, <https://doi.org/10.1126/science.aaa9932>, 2015.
- 1020 Li, Y., Brando, P. M., Morton, D. C., Lawrence, D. M., Yang, H., and Randerson, J. T.: Deforestation-induced  
 1021 climate change reduces carbon storage in remaining tropical forests, *Nat Commun*, 13, 1964,  
 1022 <https://doi.org/10.1038/s41467-022-29601-0>, 2022.

- 1023 Liu, W., Sun, F., Lim, W. H., Zhang, J., Wang, H., Shiogama, H., and Zhang, Y.: Global drought and severe  
1024 drought-affected populations in 1.5 and 2 °C warmer worlds, *Earth System Dynamics*, 9, 267–283,  
1025 <https://doi.org/10.5194/esd-9-267-2018>, 2018.
- 1026 Liu, Y., Kumar, M., Katul, G. G., Feng, X., and Konings, A. G.: Plant hydraulics accentuates the effect of  
1027 atmospheric moisture stress on transpiration, *Nat. Clim. Chang.*, 10, 691–695, <https://doi.org/10.1038/s41558-020-0781-5>, 2020.
- 1029 Ma, L., Hurtt, G. C., Chini, L. P., Sahajpal, R., Pongratz, J., Frohling, S., Stehfest, E., Klein Goldewijk, K.,  
1030 O’Leary, D., and Doelman, J. C.: Global rules for translating land-use change (LUH2) to land-cover change for  
1031 CMIP6 using GLM2, *Geoscientific Model Development*, 13, 3203–3220, <https://doi.org/10.5194/gmd-13-3203-2020>, 2020.
- 1033 Malhi, Y., Roberts, J. T., Betts, R. A., Killeen, T. J., Li, W., and Nobre, C. A.: Climate Change, Deforestation,  
1034 and the Fate of the Amazon, *Science*, 319, 169–172, <https://doi.org/10.1126/science.1146961>, 2008.
- 1035 Malhi, Y., Gardner, T. A., Goldsmith, G. R., Silman, M. R., and Zelazowski, P.: Tropical Forests in the  
1036 Anthropocene, *Annu. Rev. Environ. Resour.*, 39, 125–159, <https://doi.org/10.1146/annurev-environ-030713-155141>, 2014.
- 1038 Mamalakis, A., Randerson, J. T., Yu, J.-Y., Pritchard, M. S., Magnusdottir, G., Smyth, P., Levine, P. A., Yu,  
1039 S., and Foufoula-Georgiou, E.: Zonally contrasting shifts of the tropical rain belt in response to climate change,  
1040 *Nature Climate Change*, 11, 143–151, <https://doi.org/10.1038/s41558-020-00963-x>, 2021.
- 1041 Maslin, M. and Austin, P.: Climate models at their limit?, *Nature*, 486, 183–184,  
1042 <https://doi.org/10.1038/486183a>, 2012.
- 1043 McCormick, E. L., Dralle, D. N., Hahm, W. J., Tune, A. K., Schmidt, L. M., Chadwick, K. D., and Rempe, D.  
1044 M.: Widespread woody plant use of water stored in bedrock, *Nature*, 597, 225–229,  
1045 <https://doi.org/10.1038/s41586-021-03761-3>, 2021.
- 1046 McFarlane, N.: Parameterizations: representing key processes in climate models without resolving them,  
1047 *WIREs Climate Change*, 2, 482–497, <https://doi.org/10.1002/wcc.122>, 2011.
- 1048 Nepstad, D. C., Verssimo, A., Alencar, A., Nobre, C., Lima, E., Lefebvre, P., Schlesinger, P., Potter, C.,  
1049 Moutinho, P., Mendoza, E., Cochrane, M., and Brooks, V.: Large-scale impoverishment of Amazonian forests  
1050 by logging and fire, *Nature*, 398, 505–508, <https://doi.org/10.1038/19066>, 1999.
- 1051 van Nes, E. H., Arani, B. M. S., Staal, A., van der Bolt, B., Flores, B. M., Bathiany, S., and Scheffer, M.: What  
1052 Do You Mean, ‘Tipping Point’?, *Trends in Ecology & Evolution*, 31, 902–904,  
1053 <https://doi.org/10.1016/j.tree.2016.09.011>, 2016.
- 1054 Nijzink, R., Hutton, C., Pechlivanidis, I., Capell, R., Arheimer, B., Freer, J., Han, D., Wagener, T., McGuire,  
1055 K., Savenije, H., and Hrachowitz, M.: The evolution of root-zone moisture capacities after deforestation: a step  
1056 towards hydrological predictions under change?, *Hydrology and Earth System Sciences*, 20, 4775–4799,  
1057 <https://doi.org/10.5194/hess-20-4775-2016>, 2016.
- 1058 Nippert, J. B. and Holdo, R. M.: Challenging the maximum rooting depth paradigm in grasslands and savannas,  
1059 *Functional Ecology*, 29, 739–745, <https://doi.org/10.1111/1365-2435.12390>, 2015.
- 1060 Nof, D.: Simple Versus Complex Climate Modeling, *Eos, Transactions American Geophysical Union*, 89, 544–  
1061 545, <https://doi.org/10.1029/2008EO520006>, 2008.
- 1062 Oliveira, R. S., Dawson, T. E., Burgess, S. S. O., and Nepstad, D. C.: Hydraulic redistribution in three  
1063 Amazonian trees, *Oecologia*, 145, 354–363, <https://doi.org/10.1007/s00442-005-0108-2>, 2005.

- 1064 Oliveras, I. and Malhi, Y.: Many shades of green: the dynamic tropical forest–savannah transition zones,  
 1065 Philosophical Transactions of the Royal Society B: Biological Sciences, 371, 20150308,  
 1066 <https://doi.org/10.1098/rstb.2015.0308>, 2016.
- 1067 Parry, I. M., Ritchie, P. D. L., and Cox, P. M.: Evidence of localised Amazon rainforest dieback in CMIP6  
 1068 models, *Earth System Dynamics*, 13, 1667–1675, <https://doi.org/10.5194/esd-13-1667-2022>, 2022.
- 1069 Pascale, S., Carvalho, L. M. V., Adams, D. K., Castro, C. L., and Cavalcanti, I. F. A.: Current and Future  
 1070 Variations of the Monsoons of the Americas in a Warming Climate, *Curr Clim Change Rep*, 5, 125–144,  
 1071 <https://doi.org/10.1007/s40641-019-00135-w>, 2019.
- 1072 Piani, C., Weedon, G. P., Best, M., Gomes, S. M., Viterbo, P., Hagemann, S., and Haerter, J. O.: Statistical bias  
 1073 correction of global simulated daily precipitation and temperature for the application of hydrological models,  
 1074 *Journal of Hydrology*, 395, 199–215, <https://doi.org/10.1016/j.jhydrol.2010.10.024>, 2010.
- 1075 Poorter, L., Bongers, F., Aide, T. M., Almeyda Zambrano, A. M., Balvanera, P., Becknell, J. M., Boukili, V.,  
 1076 Brancalion, P. H. S., Broadbent, E. N., Chazdon, R. L., Craven, D., de Almeida-Cortez, J. S., Cabral, G. A. L.,  
 1077 de Jong, B. H. J., Denslow, J. S., Dent, D. H., DeWalt, S. J., Dupuy, J. M., Durán, S. M., Espírito-Santo, M. M.,  
 1078 Fandino, M. C., César, R. G., Hall, J. S., Hernandez-Stefanoni, J. L., Jakovac, C. C., Junqueira, A. B., Kennard,  
 1079 D., Letcher, S. G., Licona, J.-C., Lohbeck, M., Marín-Spiotta, E., Martínez-Ramos, M., Massoca, P., Meave, J.  
 1080 A., Mesquita, R., Mora, F., Muñoz, R., Muscarella, R., Nunes, Y. R. F., Ochoa-Gaona, S., de Oliveira, A. A.,  
 1081 Orihuela-Belmonte, E., Peña-Claros, M., Pérez-García, E. A., Piotta, D., Powers, J. S., Rodríguez-Velázquez,  
 1082 J., Romero-Pérez, I. E., Ruíz, J., Saldarriaga, J. G., Sanchez-Azofeifa, A., Schwartz, N. B., Steininger, M. K.,  
 1083 Swenson, N. G., Toledo, M., Uriarte, M., van Breugel, M., van der Wal, H., Veloso, M. D. M., Vester, H. F.  
 1084 M., Vicentini, A., Vieira, I. C. G., Bentos, T. V., Williamson, G. B., and Rozendaal, D. M. A.: Biomass  
 1085 resilience of Neotropical secondary forests, *Nature*, 530, 211–214, <https://doi.org/10.1038/nature16512>, 2016.
- 1086 Rammig, A.: Tropical carbon sinks are saturating at different times on different continents, *Nature*, 579, 38–39,  
 1087 <https://doi.org/10.1038/d41586-020-00423-8>, 2020.
- 1088 Ratnam, J., Bond, W. J., Fensham, R. J., Hoffmann, W. A., Archibald, S., Lehmann, C. E. R., Anderson, M. T.,  
 1089 Higgins, S. I., and Sankaran, M.: When is a ‘forest’ a savanna, and why does it matter?, *Global Ecology and*  
 1090 *Biogeography*, 20, 653–660, <https://doi.org/10.1111/j.1466-8238.2010.00634.x>, 2011.
- 1091 Reyer, C. P. O., Brouwers, N., Rammig, A., Brook, B. W., Epila, J., Grant, R. F., Holmgren, M., Langerwisch,  
 1092 F., Leuzinger, S., Lucht, W., Medlyn, B., Pfeifer, M., Steinkamp, J., Vanderwel, M. C., Verbeeck, H., and  
 1093 Vilella, D. M.: Forest resilience and tipping points at different spatio-temporal scales: approaches and  
 1094 challenges, *Journal of Ecology*, 103, 5–15, <https://doi.org/10.1111/1365-2745.12337>, 2015.
- 1095 Rosas, T., Mencuccini, M., Barba, J., Cochard, H., Saura-Mas, S., and Martínez-Vilalta, J.: Adjustments and  
 1096 coordination of hydraulic, leaf and stem traits along a water availability gradient, *New Phytologist*, 223, 632–  
 1097 646, <https://doi.org/10.1111/nph.15684>, 2019.
- 1098 Schenk, H. J.: Soil depth, plant rooting strategies and species’ niches, *New Phytologist*, 178, 223–225,  
 1099 <https://doi.org/10.1111/j.1469-8137.2008.02427.x>, 2008.
- 1100 Schenk, H. J. and Jackson, R. B.: The Global Biogeography of Roots, *Ecological Monographs*, 72, 311–328,  
 1101 [https://doi.org/10.1890/0012-9615\(2002\)072\[0311:TGBOR\]2.0.CO;2](https://doi.org/10.1890/0012-9615(2002)072[0311:TGBOR]2.0.CO;2), 2002.
- 1102 Schumacher, D. L., Keune, J., Dirmeyer, P., and Miralles, D. G.: Drought self-propagation in drylands due to  
 1103 land–atmosphere feedbacks, *Nat. Geosci.*, 15, 262–268, <https://doi.org/10.1038/s41561-022-00912-7>, 2022.
- 1104 Singh, C.: Rooting for forest resilience : Implications of climate and land-use change on the tropical rainforests,  
 1105 2023.

- 1106 Singh, C., Wang-Erlandsson, L., Fetzer, I., Rockström, J., and van der Ent, R.: Rootzone storage capacity  
 1107 reveals drought coping strategies along rainforest-savanna transitions, *Environ. Res. Lett.*, 15, 124021,  
 1108 <https://doi.org/10.1088/1748-9326/abc377>, 2020.
- 1109 Singh, C., van der Ent, R., Wang-Erlandsson, L., and Fetzer, I.: Hydroclimatic adaptation critical to the  
 1110 resilience of tropical forests, *Global Change Biology*, 28, 2930–2939, <https://doi.org/10.1111/gcb.16115>, 2022.
- 1111 Singh, V., Karan, S. K., Singh, C., and Samadder, S. R.: Assessment of the capability of SWAT model to  
 1112 predict surface runoff in open cast coal mining areas, *Environ Sci Pollut Res*, 30, 40073–40083,  
 1113 <https://doi.org/10.1007/s11356-022-25032-y>, 2023.
- 1114 Slik, J. W. F., Franklin, J., Arroyo-Rodríguez, V., Field, R., Aguilar, S., Aguirre, N., Ahumada, J., Aiba, S.-I.,  
 1115 Alves, L. F., K, A., Avella, A., Mora, F., Aymard C., G. A., Báez, S., Balvanera, P., Bastian, M. L., Bastin, J.-  
 1116 F., Bellingham, P. J., van den Berg, E., da Conceição Bispo, P., Boeckx, P., Boehning-Gaese, K., Bongers, F.,  
 1117 Boyle, B., Brambach, F., Brearley, F. Q., Brown, S., Chai, S.-L., Chazdon, R. L., Chen, S., Chhang, P.,  
 1118 Chuyong, G., Ewango, C., Coronado, I. M., Cristóbal-Azkarate, J., Culmsee, H., Damas, K., Dattaraja, H. S.,  
 1119 Davidar, P., DeWalt, S. J., Din, H., Drake, D. R., Duque, A., Durigan, G., Eichhorn, K., Eler, E. S., Enoki, T.,  
 1120 Ensslin, A., Fandohan, A. B., Farwig, N., Feeley, K. J., Fischer, M., Forshed, O., Garcia, Q. S., Garkoti, S. C.,  
 1121 Gillespie, T. W., Gillet, J.-F., Gonmadje, C., Granzow-de la Cerda, I., Griffith, D. M., Grogan, J., Hakeem, K.  
 1122 R., Harris, D. J., Harrison, R. D., Hector, A., Hemp, A., Homeier, J., Hussain, M. S., Ibarra-Manríquez, G.,  
 1123 Hanum, I. F., Imai, N., Jansen, P. A., Joly, C. A., Joseph, S., Kartawinata, K., Kearsley, E., Kelly, D. L.,  
 1124 Kessler, M., Killeen, T. J., Kooyman, R. M., Laumonier, Y., Laurance, S. G., Laurance, W. F., Lawes, M. J.,  
 1125 Letcher, S. G., Lindsell, J., Lovett, J., Lozada, J., Lu, X., Lykke, A. M., Mahmud, K. B., Mahayani, N. P. D.,  
 1126 Mansor, A., Marshall, A. R., Martin, E. H., Calderado Leal Matos, D., Meave, J. A., Melo, F. P. L., Mendoza,  
 1127 Z. H. A., et al.: Phylogenetic classification of the world’s tropical forests, *Proceedings of the National Academy*  
 1128 *of Sciences*, 115, 1837–1842, <https://doi.org/10.1073/pnas.1714977115>, 2018.
- 1129 Smith, C. W., Johnston, M. A., and Lorentz, S. A.: The effect of soil compaction on the water retention  
 1130 characteristics of soils in forest plantations, *South African Journal of Plant and Soil*, 18, 87–97,  
 1131 <https://doi.org/10.1080/02571862.2001.10634410>, 2001.
- 1132 Sperry, J. S. and Love, D. M.: What plant hydraulics can tell us about responses to climate-change droughts,  
 1133 *New Phytologist*, 207, 14–27, <https://doi.org/10.1111/nph.13354>, 2015.
- 1134 Staal, A., Tuinenburg, O. A., Bosmans, J. H. C., Holmgren, M., van Nes, E. H., Scheffer, M., Zemp, D. C., and  
 1135 Dekker, S. C.: Forest-rainfall cascades buffer against drought across the Amazon, *Nature Climate Change*, 8,  
 1136 539–543, <https://doi.org/10.1038/s41558-018-0177-y>, 2018.
- 1137 Staal, A., Fetzer, I., Wang-Erlandsson, L., Bosmans, J. H. C., Dekker, S. C., van Nes, E. H., Rockström, J., and  
 1138 Tuinenburg, O. A.: Hysteresis of tropical forests in the 21st century, *Nat Commun*, 11, 4978,  
 1139 <https://doi.org/10.1038/s41467-020-18728-7>, 2020.
- 1140 Stevens, B. and Bony, S.: What Are Climate Models Missing?, *Science*, 340, 1053–1054,  
 1141 <https://doi.org/10.1126/science.1237554>, 2013.
- 1142 Still, C. J., Berry, J. A., Collatz, G. J., and DeFries, R. S.: Global distribution of C3 and C4 vegetation: Carbon  
 1143 cycle implications, *Global Biogeochemical Cycles*, 17, 6-1-6–14, <https://doi.org/10.1029/2001GB001807>,  
 1144 2003.
- 1145 Stocker, B. D., Tumber-Dávila, S. J., Konings, A. G., Anderson, M. C., Hain, C., and Jackson, R. B.: Global  
 1146 patterns of water storage in the rooting zones of vegetation, *Nat. Geosci.*, 1–7, <https://doi.org/10.1038/s41561-023-01125-2>, 2023.
- 1148 Sveen, T. R., Hannula, S. E., and Bahram, M.: Microbial regulation of feedbacks to ecosystem change, *Trends*  
 1149 *in Microbiology*, 32, 68–78, <https://doi.org/10.1016/j.tim.2023.06.006>, 2024.

- 1150 Trumbore, S., Brando, P., and Hartmann, H.: Forest health and global change, *Science*, 349, 814–818,  
1151 <https://doi.org/10.1126/science.aac6759>, 2015.
- 1152 Valdes, P.: Built for stability, *Nature Geosci*, 4, 414–416, <https://doi.org/10.1038/ngeo1200>, 2011.
- 1153 Wang, E., Smith, C. J., Wang, E., and Smith, C. J.: Modelling the growth and water uptake function of plant  
1154 root systems: a review, *Aust. J. Agric. Res.*, 55, 501–523, <https://doi.org/10.1071/AR03201>, 2004.
- 1155 Wang-Erlandsson, L., Bastiaanssen, W. G. M., Gao, H., Jägermeyr, J., Senay, G. B., van Dijk, A. I. J. M.,  
1156 Guerschman, J. P., Keys, P. W., Gordon, L. J., and Savenije, H. H. G.: Global root zone storage capacity from  
1157 satellite-based evaporation, *Hydrology and Earth System Sciences*, 20, 1459–1481,  
1158 <https://doi.org/10.5194/hess-20-1459-2016>, 2016.
- 1159 Wang-Erlandsson, L., Tobian, A., van der Ent, R. J., Fetzer, I., te Wierik, S., Porkka, M., Staal, A., Jaramillo,  
1160 F., Dahlmann, H., Singh, C., Greve, P., Gerten, D., Keys, P. W., Gleeson, T., Cornell, S. E., Steffen, W., Bai,  
1161 X., and Rockström, J.: A planetary boundary for green water, *Nat Rev Earth Environ*, 3, 380–392,  
1162 <https://doi.org/10.1038/s43017-022-00287-8>, 2022.
- 1163 Wolfe, B. T., Sperry, J. S., and Kursar, T. A.: Does leaf shedding protect stems from cavitation during seasonal  
1164 droughts? A test of the hydraulic fuse hypothesis, *New Phytologist*, 212, 1007–1018,  
1165 <https://doi.org/10.1111/nph.14087>, 2016.
- 1166 Wunderling, N., Staal, A., Sakschewski, B., Hirota, M., Tuinenburg, O. A., Donges, J. F., Barbosa, H. M. J.,  
1167 and Winkelmann, R.: Recurrent droughts increase risk of cascading tipping events by outpacing adaptive  
1168 capacities in the Amazon rainforest, *Proceedings of the National Academy of Sciences*, 119, e2120777119,  
1169 <https://doi.org/10.1073/pnas.2120777119>, 2022.
- 1170 Xie, S.-P., Deser, C., Vecchi, G. A., Ma, J., Teng, H., and Wittenberg, A. T.: Global Warming Pattern  
1171 Formation: Sea Surface Temperature and Rainfall, *Journal of Climate*, 23, 966–986,  
1172 <https://doi.org/10.1175/2009JCLI3329.1>, 2010.
- 1173 Xu, C., Hantson, S., Holmgren, M., van Nes, E. H., Staal, A., and Scheffer, M.: Remotely sensed canopy height  
1174 reveals three pantropical ecosystem states, *Ecology*, 97, 2518–2521, <https://doi.org/10.1002/ecy.1470>, 2016.
- 1175 Xue, B.-L., Guo, Q., Otto, A., Xiao, J., Tao, S., and Li, L.: Global patterns, trends, and drivers of water use  
1176 efficiency from 2000 to 2013, *Ecosphere*, 6, art174, <https://doi.org/10.1890/ES14-00416.1>, 2015.
- 1177 Yang, Y., Saatchi, S. S., Xu, L., Yu, Y., Choi, S., Phillips, N., Kennedy, R., Keller, M., Knyazikhin, Y., and  
1178 Myneni, R. B.: Post-drought decline of the Amazon carbon sink, *Nat Commun*, 9, 3172,  
1179 <https://doi.org/10.1038/s41467-018-05668-6>, 2018.
- 1180 Yu, Z., Chen, X., Zhou, G., Agathokleous, E., Li, L., Liu, Z., Wu, J., Zhou, P., Xue, M., Chen, Y., Yan, W.,  
1181 Liu, L., Shi, T., and Zhao, X.: Natural forest growth and human induced ecosystem disturbance influence water  
1182 yield in forests, *Commun Earth Environ*, 3, 148, <https://doi.org/10.1038/s43247-022-00483-w>, 2022.
- 1183 Yuan, K., Zhu, Q., Riley, W. J., Li, F., and Wu, H.: Understanding and reducing the uncertainties of land  
1184 surface energy flux partitioning within CMIP6 land models, *Agricultural and Forest Meteorology*, 319, 108920,  
1185 <https://doi.org/10.1016/j.agrformet.2022.108920>, 2022.
- 1186 Zemp, D. C., Schleussner, C.-F., Barbosa, H. M. J., van der Ent, R. J., Donges, J. F., Heinke, J., Sampaio, G.,  
1187 and Rammig, A.: On the importance of cascading moisture recycling in South America, *Atmospheric  
1188 Chemistry and Physics*, 14, 13337–13359, <https://doi.org/10.5194/acp-14-13337-2014>, 2014.

- 1189 Zemp, D. C., Schleussner, C.-F., Barbosa, H. M. J., Hirota, M., Montade, V., Sampaio, G., Staal, A., Wang-  
1190 Erlandsson, L., and Rammig, A.: Self-amplified Amazon forest loss due to vegetation-atmosphere feedbacks,  
1191 Nature Communications, 8, 14681, <https://doi.org/10.1038/ncomms14681>, 2017.
- 1192 Zhang, Y., Peña-Arancibia, J. L., McVicar, T. R., Chiew, F. H. S., Vaze, J., Liu, C., Lu, X., Zheng, H., Wang,  
1193 Y., Liu, Y. Y., Miralles, D. G., and Pan, M.: Multi-decadal trends in global terrestrial evapotranspiration and its  
1194 components, Scientific Reports, 6, 19124, <https://doi.org/10.1038/srep19124>, 2016.
- 1195 Zilli, M. T., Carvalho, L. M. V., and Lintner, B. R.: The poleward shift of South Atlantic Convergence Zone in  
1196 recent decades, Clim Dyn, 52, 2545–2563, <https://doi.org/10.1007/s00382-018-4277-1>, 2019.
- 1197